ELSEVIER

Lithos 61 (2002) 55–78

LITHOS

www.elsevier.com/locate/lithos

The eclogites of the Marun–Keu complex, Polar Urals (Russia): fluid control on reaction kinetics and metasomatism during high *P* metamorphism☆

José F. Molina [a,b,*], Håkon Austrheim [b], Johannes Glodny [b,c], Anatolij Rusin [d]

[a] *Dipartimento Scienze della Terra, Università degli Studi di Milano, Via Botticelli 23, 20133 Milan, Italy*
[b] *Mineralogisk-Geologisk Museum, Sarsgate 1, N-0562 Oslo, Norway*
[c] *GeoForschungsZentrum Potsdam, Telegrafenberg C2, D-14473 Potsdam, Germany*
[d] *Institute of Geology and Geochemistry, Pochtovy per. 7, Ekaterinburg, Russia*

Received 11 September 2000; accepted 14 January 2002

Abstract

The Marun–Keu complex (Polar Urals, Russia) is a poorly known member of a group of high *P* complexes outcropping along the length of the Uralide orogen. The central and southern parts of the complex are metamorphosed at high *P*, medium *T* conditions ($T_{max} \sim 600–650$ °C and $P \sim 14–17$ kbar) and differ from its northern part and the rest of the Uralian high *P* complexes which are metamorphosed at blueschist-to-low *T* eclogite-facies conditions. The Marun–Keu complex consists of Neoproterozoic to Cambrian volcanic-sedimentary sequences with a large variety of intrusive mafic to felsic rocks. Based on the nature of protoliths and the mode of occurrence, it is distinguished: (1) eclogite-facies rocks after intrusive protoliths, which vary from metagabbros to metagranites; (2) eclogitic quartzofeldspathic gneisses; (3) metasomatic eclogites; and (4) amphibolite–eclogite alternations produced by fluid infiltration during uplift. Igneous textures and mineralogy are preserved in non-sheared, intrusive, dry rocks, whereas eclogitization may be complete along centimetre to 10-m-thick shear zones and in domains infiltrated by H_2O-dominated fluids. The most important reaction features are: (1) transformation of igneous diopside ($Na \sim 0.04–0.09$ apfu, based on 6 oxygens) into Na-rich diopside and omphacite ($Na \sim 0.24–0.45$ apfu) across microfractures and grain boundaries; (2) replacement of plagioclase by tiny aggregates of zoisite/clinozoisite + white mica + garnet ($Alm_{32–43}$, $Pyr_{7–19}$, $Gro_{38–60}$) + kyanite; and (3) double coronas of garnet and orthopyroxene at olivine–clinopyroxene and olivine–plagioclase pseudomorph interfaces and garnet coronas at clinopyroxene–plagioclase pseudomorph interfaces. Eclogitic quartzofeldspathic gneisses display a fine-scale layering of intermediate and felsic rock compositions with omphacite-bearing and omphacite-free assemblages, respectively. Oligoclase is abundant in this type of rocks, coexisting with omphacite in the intermediate rock compositions. The studied area presents a large variety of veins and metasomatic mineral sequences developing in the host-rock adjacent to the veins. High *P* minerals (garnet ($Alm_{40–60}$, $Pyr_{25–40}$, $Gro_{11–23}$), omphacite, phengite, paragonite) occur in both vein infillings and wall-rock mineral sequences, indicating that metasomatism was caused by the infiltration of out of equilibrium fluids (mostly silica-rich, alkali-rich compositions) during the eclogite-facies metamorphism. In zones of high fracture density, vein networks divide the host-rock into decimetre-scale blocks with omphacite-rich rinds

☆ Electronic supplements available on the journal's homepage: http://www.elsevier.com/locate/lithos.

* Corresponding author. Departamento de Mineralogía y Petrología, Universidad de Granada, Facultad de Ciencias, Fuentenueva s/n, 18002 Granada, Spain. Fax: +34-958-243368.

E-mail addresses: molina1@mailserver.unimi.it (J.F. Molina), hakon.austrheim@toyen.uio.no (H. Austrheim), glodnyj@gfz-potsdam.de (J. Glodny).

0024-4937/02/$ - see front matter
PII: S0024-4937(02)00070-1

replacing amphibolite cores. In contrast, metasomatic replacement of mafic eclogites by dendritic amphibole with barroisite composition (^{M4}Na ~ 0.64 apfu, based on 23 oxygens) also occurred at eclogite-facies conditions. We outline the importance of considering such metasomatic processes for the correct evaluation of $P–T–t$ metamorphic histories. The Marun–Keu complex is another example that highlights the important control exerted by fluids on reaction kinetics during high P metamorphism and further points to an important metasomatic effect of these fluids.

Keywords: Polar Urals; Marun–Keu complex; Eclogite; Fluids; Metasomatism

1. Introduction

Metamorphic rocks may store, in their mineralogy and textures, a record that can provide invaluable information on tectonic processes. Thus, eclogites, cropping out in ancient collision belts, witness the exhumation of rocks that have experienced pressures corresponding to depths of >40 km and, in the case of coesite-bearing eclogites, of >100 km. Metamorphism may change the petrophysical properties of the crust and actively influences the geodynamics of tectonic events. Evaluation of both the active role of metamorphism and the passive recording ability requires that we understand reaction kinetics behind metamorphic processes. Therefore, in order to model subduction or continental collision zones with some confidence, it is critical to unravel whether the subducted material reacts continuously or remains metastable with respect to metamorphic reactions.

Recent works have emphasized the role of fluids during eclogitization. In accordance with the work of Ahrens and Schubert (1975), several examples have been presented where the eclogitization of dry rocks is mediated by a fluid phase (e.g. Wayte et al., 1989; Rubie, 1990; Austrheim et al., 1997; Scambelluri et al., 1998; Engvik et al., 2000). Nevertheless, despite the importance of fluids during eclogitization, fluid–rock interaction processes at high P conditions are not yet well understood. Thus, large-scale fluid transport in convergent margins and collisional orogens is supported by: (1) field relationships and geochemical data in eclogitized granulite-facies rocks from Norwegian Caledonides and the Alps (e.g. Austrheim, 1987; Austrheim et al., 1997; Scambelluri et al., 1998; Jamtveit et al., 2000) and in amphibolites from Cataline Schists (California, USA) (e.g. Sorensen and Grossman, 1989; Bebout and Barton, 1993); (2) by geodynamic models for the genesis of volcanic arcs (e.g. Tatsumi, 1989; Morris et al., 1990; Plank and Langmuir, 1993); and (3) by high P experiments in mafic systems (e.g. Pawley and Holloway, 1993; Poli and Schmidt, 1995; Schmidt and Poli, 1998; Molina and Poli, 2000). In addition, a large capacity for mass transport — and, hence, for metasomatism of the mantle wedge — is suggested for such fluids owing to an increase of silicate solubility with pressure (e.g. Manning, 1998). However, restricted fluid flow, with fluid activity internally buffered by the host-rock assemblages is suggested in eclogites from the Alps based on the preservation of fine-scale chemical and isotopic heterogeneities (e.g. Selverstone et al., 1992; Philippot, 1993; Philippot and Scambelluri, 1995; Philippot et al., 1995; Scambelluri and Philippot, 2001). Therefore, further studies of veining processes in high P metamorphic terrains are essential to understand mass transfer from the subducting slab to the overlying mantle wedge at convergent margins.

The high P Marun–Keu complex (Polar Urals, Russia) contains many of the elements necessary to address the aspects of the eclogitization process outlined above. This metamorphic complex shows a wide range of bulk compositions varying from ultramafic and gabbroic to felsic rocks. This permits an analysis of the effect of the eclogite-facies metamorphism on a variety of compositional systems that together are representative of major lithotypes of the continental crust. Bodies of gabbroic and felsic rocks preserve igneous texture and mineralogy, suggesting the existence of kinetic barriers which precluded the complete transformation during metamorphism. This allows us to follow the reactions during eclogitization as have been largely studied in meta-anorthosites and metagabbros (e.g. Norwegian Caledonides, Mørk, 1985; Erambert and Austrheim, 1993; Austrheim et al., 1997; Western Italian Alps, Scambelluri et al., 1998) and metagranites (e.g. Western Italian Alps, Compag-

noni and Maffeo, 1973; Compagnoni et al., 1977; Koons et al., 1987; Biino and Compagnoni, 1992). In other areas of the Marun–Keu complex, sheared mafic rocks were fractured and infiltrated by fluids. These processes caused complete eclogitization and led to metasomatism of the host rock, suggesting an important role of the fluid phase during the eclogitization process.

In this work, we describe the field relationships observed in this geographically remote region. We also present a detailed overview of medium *T* eclogite-facies rocks from the Marun–Keu complex together with a survey of the mineral chemistry. The work further outlines the important role of fluids and metasomatic processes during the high *P* metamorphism of the Marun–Keu complex.

2. Geological setting

The Urals constitute a north–south trending Paleozoic collision belt formed by the closure of Ordovician–Silurian oceanic domains interposed between the East European craton and an assemblage of Sibe-

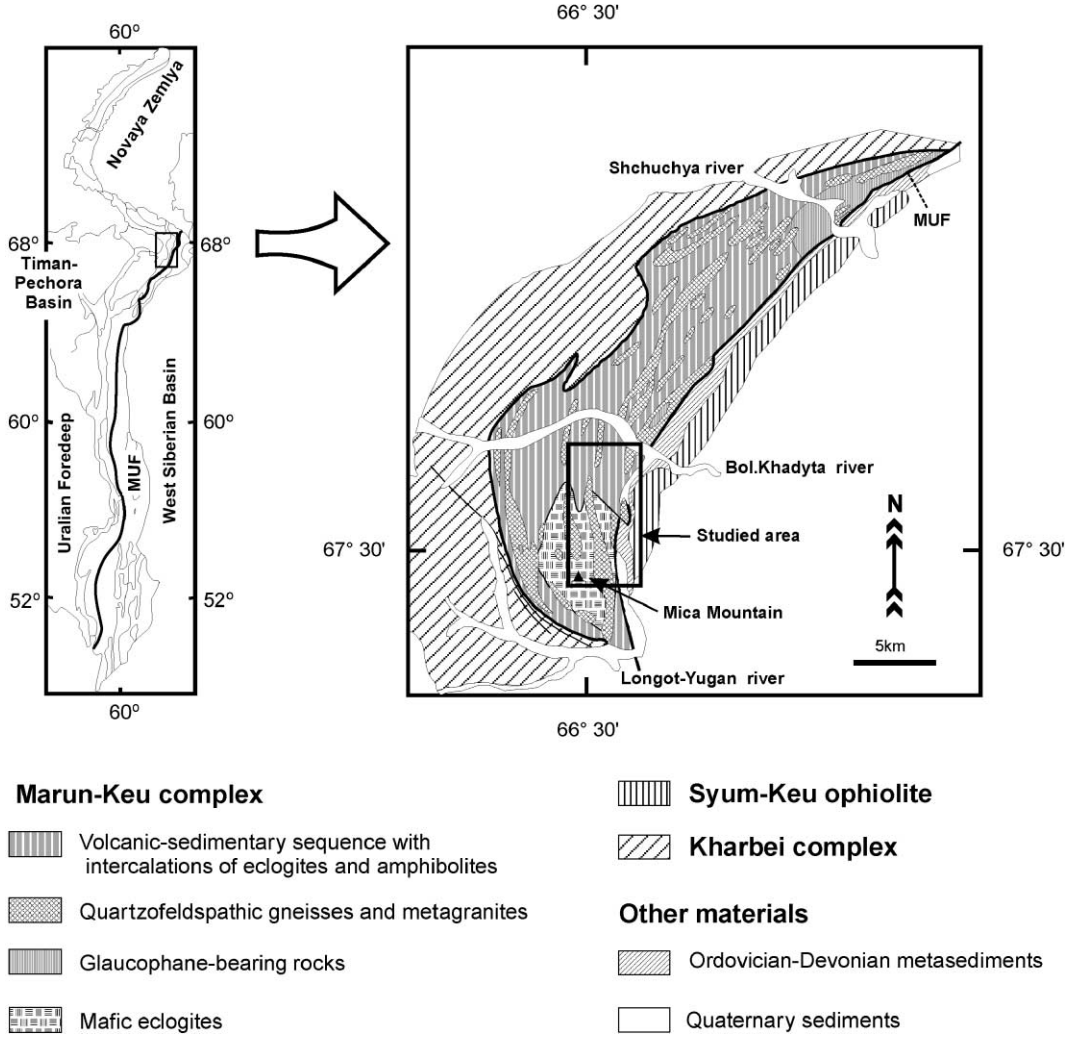

Fig. 1. Geological map of the Marun–Keu complex modified after Udovkina (1971) and Bezzubtsev et al. (1986).

Table 1
Samples analyzed in this study

Reference	Rock type[a]	GPS coordinates	Mineralogy[b]	Notes[b]
J-6	MGb	67.29.70 N, 66.32.01 E	Omp, Na-rich Di, Opx, Gar, Ca Amp, Zo/Cz, Pheng, Ky, Q, Ru	Coronitic texture, intensive transformation to eclogite-facies assemblages
J-9	ME	67.29.70 N, 66.32.01 E	Vein: Gar + Di Wall-rock band: Omp + Gar	Vein Gar with grossular-andradite composition Alm-rich Gar in the wall-rock band (Alm_{52} Pyr_{11} Gro_{36})
J-12	ME	67.29.70 N, 66.32.01 E	Vein: Q, Pheng, Omp, Gar, Na–Ca Amp, Ru; Eclogite: Omp, Gar, Na–Ca Amp, Pg, Pheng, Q, Ru; Amphibolite: Gar, Na–Ca Amp, Pg, Pheng, Q, Ru	Block in Q-Wm vein with eclogite rind surrounding amphibolite core
J-24	QFG	67.28.65 N, 66.36.13 E	Q, Cz/Ep, Plg, Gar, Pheng, Ap, Ru	Intercalated with J-25
J-25	QFG	67.28.65 N, 66.36.13 E	Q, Cz/Ep, Ca Amp, Omp, Plg, Gar, Pheng, Ap, Ru	Intercalated with J-24
PU-10A	MGr	67.34.11 N, 66.38.80 E	Q, Plg, K–Fd, Bio, Gar, Wm, Ilm, Ep, All	Scarcely deformed
PU-11	ME	67.34.11 N, 66.38.80 E	Vein: Gar, Omp, Amp, Wm, Q, Zo (All cores) Mineral band: Gar + Sph Host rock: Gar, Omp, Wm, Ru, Q	Gar + Sph mineral bands adjacent to a high *P* vein Gar shows ca Gro_{20}, contrasting with J-9 Dendritic Amp replacing host-rock eclogite
PU-12	MGr	67.34.85 N, 66.39.92 E	Q, Plg, K–Fd, Bio, Gar, Wm, Ilm, Ep, All	Scarcely deformed
PU-31a	AAEA	67.33.44. N, 66.37.04 E	Gar, Amp, Ab, Ep, Pheng, Q, Sph, Ap	Amphibolite replacing eclogite PU-31e2 with evidence of no metasomatism
PU-31e2	EAEA	67.33.44. N, 66.37.04 E	Gar, Amp, Cpx, Ep, Pheng, Q, Ru, Ap	Eclogite replaced by amphibolite PU-31a with evidence of no metasomatism
PU-34	ME	67.33.44. N, 66.37.04 E	Eclogite: Omp, Gar, Amp, Pheng, Q, Ru, Cl–Ap Amphibolite: Amp, Omp, Q, Ru, Cc, S	Block in Q-Wm vein with eclogite rind surrounding amphibolite core. Omp + Gar + Amp veins crosscut the amphibolite core
PU-49	ME	67.30.20 N, 66.34.30 E	Vein: Q + Omp + K–Fd Wall-rock: band 1: Omp; band 2: Ca Amp+Q; band 3: Opx + Gar + Ca Amp + Bio + Ilm	Omp band adjacent to the vein followed outward by Amp, and Opx + Gar + Bio mineral bands
PU-50	MGr	67.30.00 N, 66.33.55 E	Q, K-Fd, Plg, Zo/Cz, Gar, Wm, Ilm	Intensively deformed
PU-55	ME	67.29.72 N, 66.31.98 E	Gar, Omp, Amp, Wm, Q, Ru	Veins of dendritic Amp replacing eclogite
PU-58	MQD	67.29.72 N, 66.31.98 E	Q, Zo/Cz, Ca Amp, Omp, Na–Di, Wm, Sph	Scarcely deformed. Interstitial Q among euhedral pseudomorphs after Plg
PU-62-2	MGb	67.29.04 N, 66.29.61 E	Ol, Opx, Di, Omp, Na-rich Di, Opx, Gar, Ca Amp, Zo/Cz, Pheng, Bio, Ky, Q, Ru, Cr–Sp, Ilm, S, Cl–Ap	Coronitic textures
PU-62-3	MGb	67.29.04 N, 66.29.61 E	Ol, Opx, Di, Bio, Zo/Cz, Pheng, Omp, Na-rich Di, Opx, Gar, Ca Amp, Ky, Q, Ru, Ilm, S, Cl–Ap	Coronitic textures

[a] AAEA, amphibolite in amphibolite–eclogite alternations; EAEA, eclogite in amphibolite–eclogite alternations; MDo, metadolerite; MGb, metagabbro; MGr, metagranite; MQD, metaquartz–diorite; ME, metasomatic eclogites; QFG, quartzofeldspathic gneisses.

[b] Ab, albite; All, allanite; Amp, amphibole; Ap, apatite; Bio, biotite; Cc, calcite; Cz, clinozoisite; Di, diposide; Ep, epidote; Fd, feldspar; Gar, garnet; Ilm, ilmenite; Ol, olivine; Omp, omphacite; Opx, orthopyroxene; Pg, paragonite; Pheng, phengite; Plg, plagioclase; Q, quartz; Ru, rutile; S, sulphides; Sp, spinel; Sph, sphene; Wm, white mica; Zo, zoisite.

rian–Kazakhian island-arc and continental terrains (e.g. Savelieva and Nesbitt, 1996; Brown et al., 1998).

One of the most outstanding features of the Uralide orogen is the Main Uralian Fault (MUF), which represents the principal suture zone of the Urals. To the east of the MUF, ophiolitic, mafic–ultramafic complexes occur, interpreted as remnants of suprasubduction-zone mantle-wedge and of pre-Uralian oceanic crust (e.g. Savelieva and Saveliev, 1992; Savelieva and Nesbitt, 1996; Fershtater et al., 1997). To the east of the ophiolite belt, island arc type rocks as well as post-kinematic granitoids are found (e.g. Bea et al., 1997; Fershtater et al., 1997; Montero et al., 2000).

To the west of the MUF, numerous eclogite-facies complexes appear along the orogen defining a discontinuous, but persistent high *P* metamorphic belt (e.g. Dobretsov and Sobolev, 1970; Sobolev et al., 1986; Ernst et al., 1995). In these complexes, the most widespread mineral assemblages are characterized by the presence of glaucophane (e.g. Sobolev et al., 1986; Beane et al., 1995; Gómez-Pugnaire et al., 1997; Hetzel et al., 1998; Schulte and Blümel, 1999), suggesting cold thermal regimes during the high *P* metamorphism.

The Marun–Keu complex in the Polar Urals (approximately 67°N, 66°E) (Fig. 1) with an area of ~300 km^2 represents the northernmost part of the Uralian high *P* metamorphic belt. It has been described by, e.g., Udovkina (1971), Dobretsov and Sobolev (1984), Sobolev et al. (1986), Savelieva and Nesbitt (1996), Lennykh et al. (1997), Austrheim (1998) and Glodny et al. (in preparation). The com-

Table 2
Major-(wt.%) and trace-(ppm) element composition of representative rock types from the Marun–Keu complex[a]

Label	PU-62	PU-63C	PU-51	PU-58	PU-50	J-24	J-25	J-1G	J-30	PU-49D	J-32CC	PU-31-B2	PU-31-D-2B
Rock type[b]	MGb	MGb	MDo	MQD	MGr	QFG	QFG	ME vein	ME vein	ME amphibolite	ME eclogite	AAEA	EAEA
SiO_2	47.24	51.14	48.14	61.66	72.36	69.30	55.92	61.01	71.77	49.27	49.78	51.65	52.66
TiO_2	0.17	0.24	1.15	0.92	0.24	0.56	0.83	2.26	0.46	0.18	0.94	1.13	1.19
Al_2O_3	21.42	16.56	19.06	18.63	15.00	15.46	17.76	8.93	13.14	10.08	16.38	14.65	14.60
Fe_2O_3	6.91	7.98	10.80	4.86	3.06	4.07	9.51	4.85	3.76	12.23	9.64	11.91	11.86
MnO	0.11	0.15	0.19	0.07	0.02	0.06	0.13	0.04	0.06	0.26	0.17	0.19	0.19
MgO	9.61	10.45	5.83	1.82	0.43	1.02	3.91	7.20	1.39	14.94	7.15	6.76	6.77
CaO	12.23	11.38	9.67	5.50	1.90	3.69	7.24	10.34	5.02	9.17	9.03	10.82	10.67
Na_2O	2.08	1.82	3.56	5.07	1.91	2.77	2.19	4.72	0.54	2.28	3.49	2.43	2.04
K_2O	0.11	0.16	1.60	1.44	3.17	1.93	1.59	0.04	2.01	0.43	2.02	0.47	0.47
P_2O_5	0.02	0.02	0.16	0.24	0.15	0.14	0.13	0.24	0.17	0.07	0.04	0.16	0.16
LOI	0.24	0.03	0.42	0.49	1.28	1.00	0.54	0.09	1.06	1.35	0.93	0.53	bdl
Total	100.14	99.92	100.58	100.70	99.52	100.02	99.74	99.74	99.39	100.26	99.57	100.69	100.57
Rb	6	12	50	73	77	76	67	7	56	16	60	21	19
Sr	267	147	371	607	326	353	321	75	437	129	75	200	193
V	90	131	299	74	24	38	196	260	25	40	277	226	197
Cr	712	1430	344	295	237	324	311	816	84	1243	565	412	458
Co	43	57	33	14	5	6	21	18	8	68	38	43	49
Ni	205	343	18	14	6	9	21	137	17	499	113	68	71
Y	11	12	31	19	26	24	31	11	41	17	29	33	33
Zr	22	28	105	196	269	249	136	31	388	36	120	101	105
Nb	bdl	bdl	4	11	4	10	5	12	8	1	7	4	4
Pb	bdl	7	7	14	14	8	7	6	18	6	bdl	bdl	6
Th	2	bdl	bdl	7	39	14	bdl	bdl	13	3	3	3	bdl
U	bdl	3	3	6	4	3	3	2	4	2	3	bdl	3

bdl: Below detection limit.

[a] Analyses performed by XRF at the Geological Institute (University of Oslo). Other analyses used in diagrams and discussion are in Glodny et al. (in preparation).

[b] MDo, metadolerite; MGb, metagabbro; MGr, metagranite, MQD, metaquartz–diorite; ME, metasomatic eclogites; QFG, quartzo-feldspathic gneisses; AAEA, amphibolite in amphibolite–eclogite alternations; EAEA, eclogite in amphibolite–eclogite alternations.

plex represents subducted continental crust of the pre-Uralian East European passive margin (Glodny et al., in preparation), metamorphosed during subduction and collision processes at ~360–355 Ma (Glodny et al., 2000). The Marun–Keu complex consists of Neoproterozoic to Cambrian volcanic–sedimentary sequences with a large variety of felsic to mafic intrusive rocks. With respect to the Uralian structures, the complex forms a thrust sheet with low-grade metasedimentary sequences of the Kharbei complex in the footwall, and oceanic and mantle rocks of the Syum–Keu ophiolite in the hangingwall (Udovkina, 1971; Savelieva and Nesbitt, 1996; Scarrow et al., 2001). Based on whole-rock elemental chemistry, Sr–Nd isotopic data and U–Pb single-zircon dating, Glodny et al. (in preparation) consider the protoliths of the Marun–Keu complex as a fragment of juvenile Timanian crust with island–arc signature, formed and accreted to the East European craton during the Timanian (Late Neoproterozoic III) orogeny.

The Marun–Keu complex represents a unique case with blueschist- and medium *T* eclogite-facies rocks (Udovkina, 1971; Dobretsov and Sobolev, 1984; Sobolev et al., 1986). In the northern part of the complex, near the Shchuchya River (Fig. 1), glaucophane metabasites alternate with garnet–crossite quartzites and

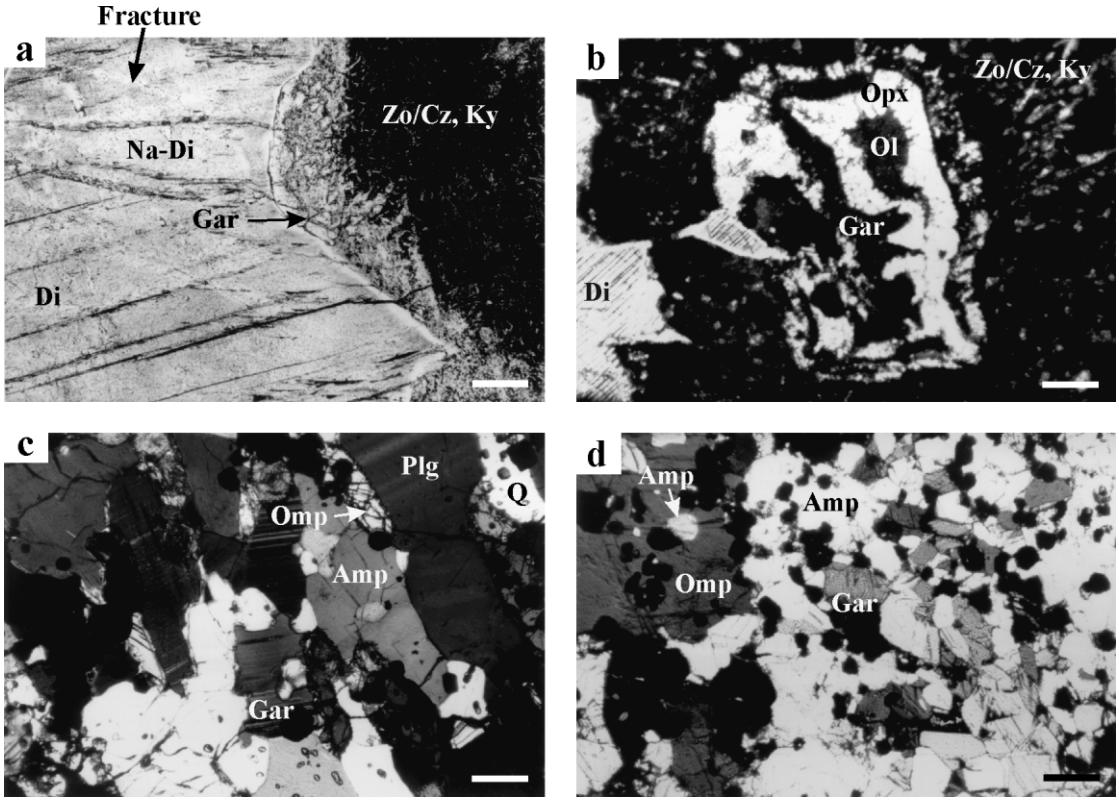

Fig. 2. Photomicrographs of high P rocks from the Marun–Keu complex. (a) Partially eclogitized gabbro with dark igneous diopside replaced by colourless Na-rich diopside and omphacite along fractures and grain boundaries. Note sharp garnet–clinopyroxene interface and dendritic garnet across zoisite/clinozoisite + kyanite aggregates after plagioclase. Sample PU-62-2. Scale bar 0.26 mm. (b) Partially eclogitized gabbro with orthopyroxene corona adjacent to igneous olivine and garnet coronas at the contact with igneous clinopyroxene and zoisite/clinozoisite + kyanite aggregates after plagioclase. Sample PU-62-3. Scale bar 0.26 mm. (c) Foliated matrix in QFG. Note sharp omphacite–plagioclase interfaces evidencing stability of plagioclase during the eclogite-facies metamorphism. Sample J-25. Scale bar 0.26 mm. (d) Coarse omphacite replacing decussate aggregates of amphibole + garnet + mica at the contact between eclogite and amphibolite bands in ME. Note abundant inclusions of garnet and amphibole in clinopyroxene. Sample J-12. Scale bar 0.26 mm.

metagraywackes, suggesting cold thermal regimes (i.e. similar to those of HP complexes in the Middle and Southern Urals). However, in the central and southern parts of the Marun–Keu complex, quartzofeldspathic gneisses, garnet amphibolites and barroisite eclogites were formed under warmer thermal regimes (Udovkina, 1971; Dobretsov and Sobolev, 1984; Sobolev et al., 1986).

3. Eclogite-facies rocks of the Marun–Keu complex

The studied area comprises the central and southern part of the Marun–Keu complex (Fig. 1). Most of our observations and samples were collected in river valleys, where nearly continuous, kilometre-sized outcrops occur.

Based on the nature of protoliths and mode of occurrence the investigated rocks are divided into four types: (1) eclogite-facies rocks formed from igneous protoliths; (2) eclogitic quartzofeldspathic gneisses (hereafter QFG); (3) metasomatic eclogites (hereafter ME); (4) amphibolite–eclogite alternations (hereafter AEA) (see Table 1 for location of the studied samples, and Table 2 for representative whole-rock analyses).

3.1. Eclogite-facies rocks formed from intrusive protoliths

The plutonic rocks of the Marun–Keu complex comprise websterites, gabbros, diorites, quartz diorites, granites, and doleritic dikes. This suite was variably metamorphosed at medium *T* eclogite-facies conditions. Partially eclogitized troctolite gabbros and granites are well exposed in Mica Mountain and near Bol. Khadyta River, respectively (Fig. 1).

Except doleritic dikes, all intrusive rocks are subalkaline, with significantly high alkali contents in metaquartz–diorites (Table 2). Notably, metagabbros can present up to ~22 wt.% Al_2O_3 and ~14 wt.% CaO in the more leucocratic varieties, suggesting accumulation of plagioclase. Less transformed granites, which still preserve igneous feldspar and brown biotite, present ~3.4–5.5 wt.% Na_2O and ~2.5–5

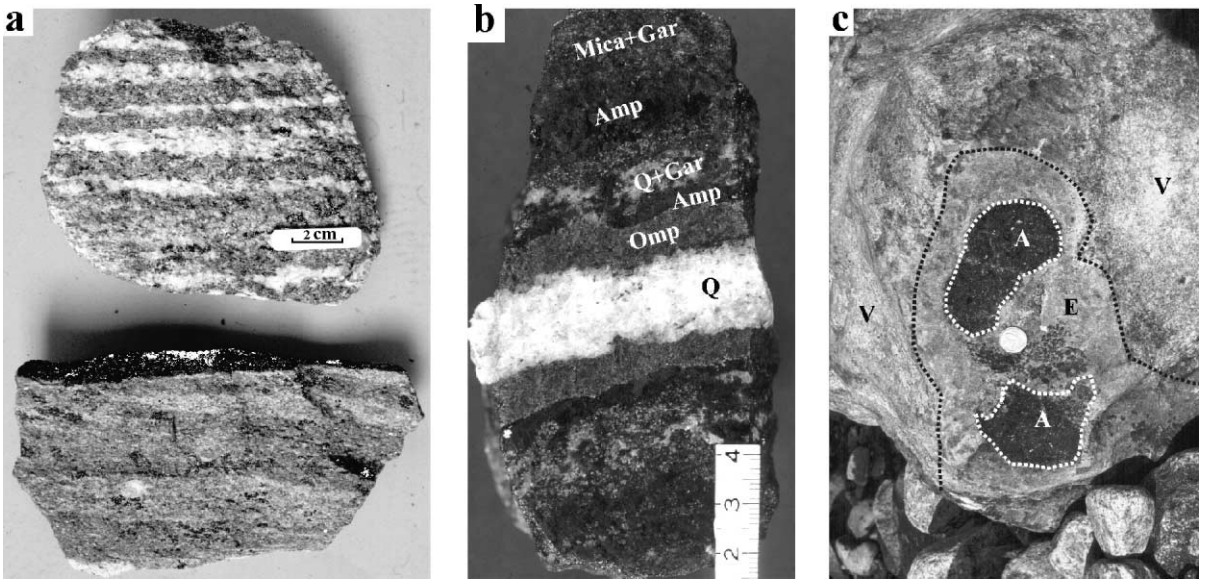

Fig. 3. Photographs of handspecimens of high *P* rocks from the Marun–Keu complex. (a) Quartzofeldspathic rocks (samples J-24 (upper) and J-25 (lower)) with a coarse compositional banding defined by quartz–plagioclase-, and omphacite–amphibole-rich layers. Note leucocratic layer in J-24 consisting of almost pure quartz + plagioclase aggregates. Note also, in both samples, a millimetre-scale banding caused by small modal variations in quartz, plagioclase and ferromagnesian mineral phases. (b) Symmetric mineral banding parallel to a quartz-rich vein. Note monomineralic band of omphacite adjacent to the vein. (c) Block included in a quartz–mica vein (V), with evidence of metasomatism consisting of the development of an eclogite rind (E) surrounding a darker amphibolite (A) core.

wt.% K_2O, whereas sheared granites, which contain aggregates of very tiny white mica and zoisite/clinozoisite after feldspar and abundant garnet and phengite, present lower Na_2O, but similar K_2O (see PU-50 in Table 2).

The eclogitization of gabbroic rocks is controlled by deformation and availability of fluids. In the troctolite gabbros from Mica Mountain, the gabbro-to-eclogite transformation is more advanced and locally ran to completion in centimetre to 10-m-thick shear zones, whereas Austrheim (1998) presented an example of eclogitization following fluid fronts (Fig. 4d in Austrheim, 1998). In the less reacted gabbros, magmatic olivine, enstatite, diopsidic clinopyroxene, Fe–Ti oxides, Cr-spinel, sulphides and brown biotite may be still preserved as cores to corona structures. The replacement textures are similar to those described by Mørk (1985) in Sunnmøre, Western Norway, and Gilotti and Elvevold (1998) in Ambolten, NE Greenland. Igneous olivine and clinopyroxene are replaced by orthopyroxene coronas and by Na-rich diopside and omphacite, respectively, implying exchange of Si, Mg and Fe with the intergranular medium in olivine domains and of Si, Al, Ca and Na in clinopyroxene domains. These mineral replacements occur along grain boundaries and microfractures (Fig. 2a, b), evidencing fast mass transport across the intergranular medium (probably due to the presence of a fluid film) and negligible intracrystalline diffusion. Plagioclase is replaced by aggregates of tiny zoisite/clinozoisite, garnet and kyanite with scarce quartz, omphacite and amphibole and very rare phengite and albite. Single garnet coronas arise at clinopyroxene–plagioclase pseudomorph interfaces (Fig. 2a), whereas at the interfaces between olivine and plagioclase pseudomorphs, and olivine and clinopyroxene, double coronas of orthopyroxene (adjacent to olivine) and garnet (next to plagioclase pseudomorphs and clinopyroxene) occur (Fig. 2b). Remarkably, the garnet coronas present sharp contacts with orthopyroxene and clinopyroxene and irregular, locally dendritic, contacts with plagioclase pseudomorphs (Fig. 2a, b), which may suggest rapid growth or limited mass transport across the grain boundaries of the mineral aggregates after plagioclase. Notably, at plagioclase pseudomorph–Cr-spinel interfaces, coronas of garnet and green kyanite occur, with Cr_2O_3 contents of up to 6 and 9 wt.%, respectively, which are even higher than those reported in kyanite from high *P* ultramafic rocks from the Cabo Ortegal complex (NW Spain) (Gil-Ibarguchi et al., 1991). In the advanced stages of transformation, Cr-rich corundum develops after Cr-spinel.

3.2. Eclogitic quartzofeldspathic gneisses

Banded gneisses are well exposed at a small creek in the southern part of the complex (67.28.65N, 66.36.13E). The sequence shows a centimetre-to-decimetre-scale compositional banding made of an interlayering of omphacite (+amphibole)-bearing and

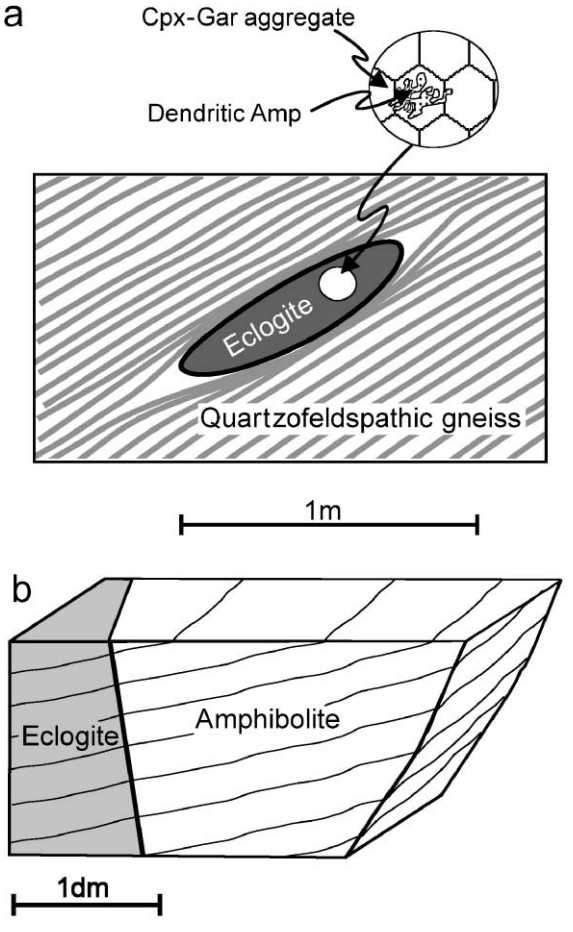

Fig. 4. Schematic field relationships in high *P* rocks from the Marun–Keu complex. (a) QFG with blocks of mafic eclogites. (b) Sharp contact between eclogites and amphibolites transecting the foliation with no evidence of metasomatism.

omphacite-free assemblages (Fig. 3a), which is parallel to a foliation defined by the preferred orientation of clinozoisite, amphibole, omphacite and phengite (see samples J-24 and J-25 in Table 1 for a description of the mineral assemblages). In addition, rare decimetre-to-metre-scale blocks of mafic eclogites containing centimetre-sized patches of dendritic amphibole (see next section about metasomatic eclogites) (Fig. 4a) also occur enclosed in these banded sequences.

The quartzofeldspathic gneisses with omphacite assemblages present intermediate compositions with higher Fe_2O_3, MgO and CaO contents than those with omphacite-free assemblages (Table 2), suggesting that the differences in the bulk composition may be the factor controlling the occurrence of omphacite in these rocks as will be discussed later.

It is also important to remark the presence of coarse-grained plagioclase with straight grain boundaries towards omphacite (Fig. 2c), which provides an evidence for the coexistence of plagioclase and omphacite in the QFG during the eclogite-facies stage.

Table 3
Representative clinopyroxene analyses

Label	PU62-3-6	PU62-2-1	PU62-2-2b	PU58-1px	PU58-2px	J25-2-2	J12-1-cg-1	PU34D-cg-2	PU55-1px	J9-1px	J9-2px	PU31-e2-1
Rock-type[a]	MGb	MGb	MGb	MQD	MQD	QFG	ME	ME	ME	ME	ME	EAEA
Texture	Relic	Ophitic cpx core	Ophitic cpx rim	Rim	Plg pseud.	Matrix	Eclogite rind	Vein	Eclogite	Ca-rich vein	Contact vein	Core
wt.%												
SiO_2	52.74	54.73	54.21	55.97	53.72	54.41	55.31	56.01	55.78	52.35	54.96	56.23
TiO_2	0.35	0.07	0.19	0.27	0.12	0.27	0.17	0.17	0.19	0.29	0.05	0.04
Al_2O_3	2.59	6.88	11.05	11.66	7.71	10.94	10.86	11.58	11.49	0.98	6.99	9.25
Cr_2O_3	0.23	0.00	0.00	0.19	0.03	0.10	0.04	0.06	0.03	0.01	0.01	0.06
NiO	0.00	0.01	0.05	0.00	0.00	0.00	0.00	0.00	0.05	0.05	0.00	0.00
FeO_T	6.39	4.18	3.68	7.23	7.55	5.85	3.78	4.17	3.72	12.35	7.87	4.39
MnO	0.18	0.05	0.00	0.10	0.00	0.08	0.03	0.04	0.05	0.89	0.09	0.00
MgO	14.36	11.06	8.66	6.40	9.30	8.24	8.79	7.88	8.72	9.09	8.72	9.37
CaO	23.07	18.22	15.91	12.02	17.77	14.72	14.26	12.84	14.57	22.78	16.58	15.33
Na_2O	0.47	3.92	5.66	7.74	4.17	6.03	6.59	7.33	6.35	1.31	5.00	5.99
K_2O	0.01	0.00	0.01	0.04	0.04	0.01	0.01	0.04	0.00	0.00	0.00	0.01
Total	100.40	99.12	99.42	101.62	100.40	100.65	99.84	100.12	100.94	100.10	100.29	100.68
Si	1.940	1.991	1.947	1.968	1.947	1.939	1.966	1.979	1.962	1.986	1.990	1.990
Ti	0.010	0.002	0.005	0.007	0.003	0.007	0.004	0.004	0.005	0.008	0.001	0.001
Al	0.112	0.294	0.467	0.484	0.330	0.459	0.454	0.482	0.477	0.044	0.299	0.387
Cr	0.007	0.000	0.000	0.005	0.001	0.003	0.001	0.002	0.001	0.000	0.000	0.002
Ni	0.000	0.000	0.001	0.000	0.000	0.000	0.000	0.000	0.001	0.002	0.000	0.000
Fe_T	0.196	0.127	0.110	0.213	0.229	0.174	0.112	0.123	0.110	0.393	0.239	0.130
Mn	0.006	0.002	0.000	0.003	0.000	0.002	0.001	0.001	0.002	0.029	0.003	0.000
Mg	0.786	0.599	0.463	0.336	0.503	0.437	0.465	0.415	0.458	0.515	0.472	0.495
Ca	0.908	0.709	0.611	0.454	0.691	0.561	0.542	0.486	0.550	0.928	0.644	0.582
Na	0.034	0.276	0.394	0.528	0.293	0.416	0.454	0.502	0.434	0.096	0.352	0.412
K	0.001	0.000	0.001	0.002	0.002	0.001	0.001	0.002	0.000	0.000	0.000	0.000
^{IV}Al	0.060	0.009	0.053	0.032	0.053	0.061	0.034	0.018	0.038	0.014	0.010	0.010
^{VI}Al	0.053	0.285	0.415	0.452	0.277	0.398	0.420	0.464	0.440	0.030	0.289	0.377
Fe^{3+}	0.015	0.000	0.022	0.091	0.064	0.061	0.058	0.047	0.021	0.064	0.069	0.042
Fe^{2+}	0.181	0.127	0.088	0.122	0.166	0.113	0.054	0.076	0.088	0.329	0.169	0.089

[a] MGb, metagabbro; MQD, metaquartz–diorite; ME, metasomatic eclogites; QFG, quartzofeldspathic gneisses; EAEA, eclogite in amphibolite–eclogite alternations.

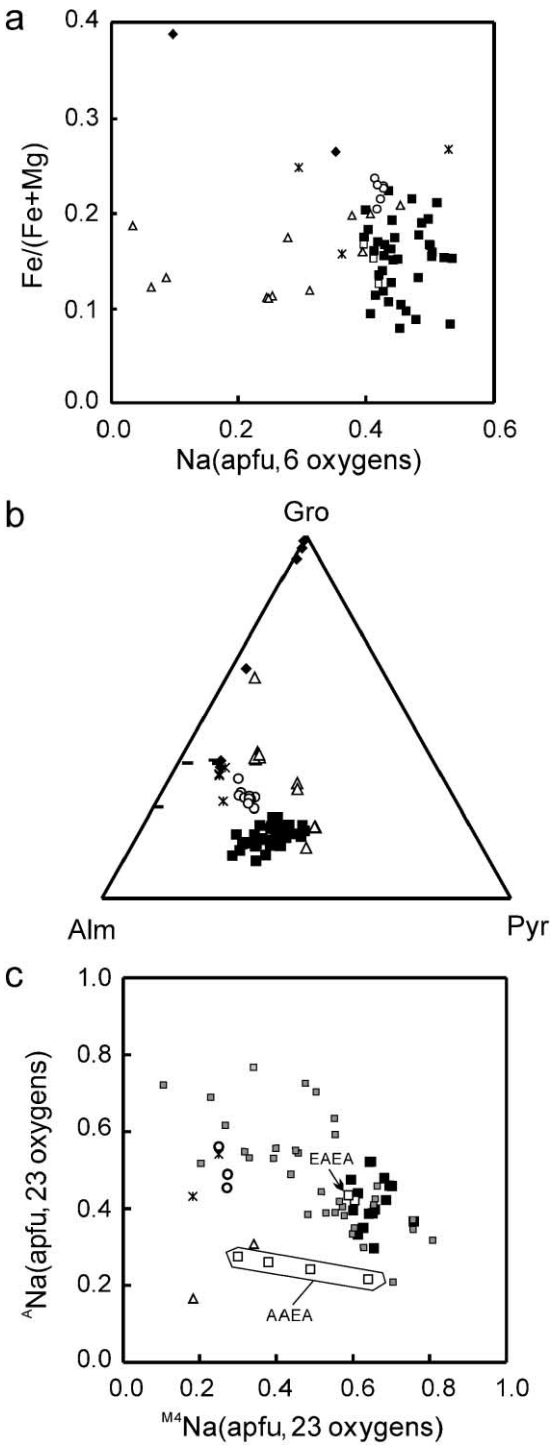

Fig. 5. Mineral compositions in rocks from the Marun–Keu complex. (a) Clinopyroxene composition. (b) Garnet composition in the Pyr–Alm–Gro diagram. (c) Amphibole composition. AAEA, amphibolite in amphibolite–eclogite alternations; EAEA, eclogite in amphibolite–eclogite alternations. Symbols: open triangles, metagabbros; open circles, QFG; asterisk, metaquartz–diorites; stripe, metagranites; open squares, eclogites alternating with amphibolites; filled squares, ME and veins, except Cl-bearing amphibole in PU-34 (small grey squares) and calcium-rich veins (filled diamonds).

3.3. Metasomatic eclogites

The Marun–Keu complex is characterized by the abundance of veins with alteration haloes in the wall rock. The most abundant veins are quartz-rich, with variable amounts of white mica (mostly phengite, but also paragonite), almandine-rich garnet, omphacite and amphibole and rare rutile, sphene or Cl–apatite (e.g. PU-34 in Table 1). Locally, monomineralic garnet and omphacite veins also occur. In addition, there are also grossular–andradite + diopside veins (J-9 in Table 1). In the wall rocks adjacent to the veins, a large variety of mineral sequences (note samples PU-11, PU-49 and J-9 in Table 1) develop in bands parallel to the veins (e.g. see symmetrical bands in Fig. 3b). Remarkably, omphacite + almandine-rich garnet assemblages are usually present in these mineral sequences (even in the wall rock of grossular–andradite + diopside veins (J-9 in Table 1)), suggesting that fluid circulation and growth of mineral bands in the wall rocks occurred during the eclogite-facies metamorphism.

In zones of high fracture density, vein networks divide the host-rock into decimetre-scale blocks. The blocks normally display an amphibolite core separated from the vein by an 1–2-cm-thick omphacite-rich rind. The eclogite band grades into the quartz–mica vein (Fig. 3c), suggesting the precipitation in the vein of material dissolved from the host-rock during fluid infiltration. However, the boundary between the eclogite rind and the amphibolite can be sharp, with coarse omphacite replacing decussate aggregates of amphibole + garnet + mica (Fig. 2d). In the amphibolite cores, omphacite may be absent or may coexist with am-phibole (e.g. see J-12 and PU-34, respectively, in Table 1), suggesting that the assemblages in the central part of the blocks could also be formed at eclogite-facies conditions.

Contrasting with the blocks previously described, dendritic amphibole related to high *P* veins (e.g. PU-11 in Table 1) can replace almandine-rich garnet + omphacite assemblages from mafic rocks. This amphibole presents numerous inclusions of garnet and omphacite from the rock-matrix assemblage and, locally, is aligned along planes emanating out from the vein into the eclogite. These textural evidences and the presence of omphacite in the vein suggest that the replacement of the rock-matrix assemblage by the dendritic amphibole was caused by the infiltration of fluids derived from the vein during the eclogite-facies metamorphism.

The mineral infillings previously reported suggest that the fracture fluids were very heterogeneous, with silica-dominated, and calcium-dominated compositions. Representative compositions of quartz-dominated veins and alterations haloes are displayed in Table 2. Alkali contents in the quartz veins are very variable with Na_2O and K_2O ranging from 0.5 to 4.8 wt.% and from < 0.1 to 3.0 wt.% K_2O, respectively. The presence of rutile, sphene and Cl–apatite in the vein infillings also evidences the transport of Ti, P and Cl by the high *P* fluids (see also Scambelluri and Philippot (2001) for further discussions). Thus, it is interesting to note that TiO_2 can reach up to 2.26 wt.% (J-1G in Table 2), whereas the contents of trace elements like Cr, V and Zr, which usually are immobile in other environments, can be also high in the veins.

Table 4
Representative garnet analyses. An extensive dataset can be found on the journal's homepage http://www.elsevier.com/locate/lithos under "Electronic Supplements"

Label	PU-62-3-7	PU-62-2-11	PU-62-2-4	PU-50-1g	PU-50-2g	J-25-2-16	PU-31e2-3	PU-31e2-4	PU-31-a-2	J-12-1-5	J-12-1-19	J-9-2g	J-9-1g
Rock-type[a]	MGb	MGb	MGb	MGr	MGr	QFG	EAEA	EAEA	AAEA	ME	ME	ME	ME
Texture	After Plg	Opx domain	Core in gar corona	Near ilm	Rim in foliated matrix	Rim	Core	Rim	Core	Core in eclogite	Core in amphibolite	Near Plg	Ca-rich vein
wt.%													
SiO_2	39.06	39.56	39.28	37.16	38.57	38.89	38.86	38.77	39.57	39.39	39.66	38.57	38.94
TiO_2	0.12	0.08	0.03	0.07	0.03	0.03	0.09	0.09	0.12	0.08	0.02	0.17	0.22
Al_2O_3	21.22	21.77	21.39	19.48	20.96	21.52	21.4	21.16	21.51	21.64	21.94	20.88	17.31
Cr_2O_3	0.44	0.28	0.06	0.00	0.01	0.00	0.00	0.06	0.04	0.03	0.01	0.01	0.03
NiO	0.00	0.03	0.00	0.00	0.00	0.00	0.07	0.00	0.01	0.06	0.01	0.05	0.00
FeO_T	15.41	20.43	19.23	34.22	23.92	24.3	22.16	24.19	19.83	21.11	22.82	23.71	8.49
MnO	0.18	0.74	0.80	0.48	0.66	0.30	0.61	0.48	0.44	0.79	1.06	0.32	2.35
MgO	1.89	11.41	4.99	0.28	2.45	6.10	5.33	6.09	4.98	9.29	9.48	2.74	0.18
CaO	22.90	5.19	13.99	9.14	13.12	9.72	11.3	8.33	12.85	6.83	5.26	12.7	32.17
Na_2O	0.03	0.07	0.03	0.05	0.03	0.04	0.01	0.01	0.05	0.04	0.05	0.03	0.04
K_2O	0.01	0.01	0.00	0.01	0.02	0.02	0.00	0.00	0.00	0.02	0.00	0.06	0.00
Total	101.28	99.56	99.8	100.89	99.78	100.94	99.84	99.19	99.41	99.28	100.33	99.25	99.72
Si	2.993	3.000	3.030	3.008	3.032	2.994	3.009	3.022	3.050	3.018	3.016	3.039	3.008
Ti	0.007	0.005	0.002	0.004	0.002	0.002	0.005	0.005	0.007	0.005	0.001	0.010	0.013
Al	1.913	1.943	1.942	1.862	1.945	1.950	1.956	1.948	1.958	1.951	1.963	1.943	1.579
Cr	0.027	0.017	0.004	0.000	0.001	0.000	0.000	0.004	0.003	0.002	0.001	0.001	0.002
Ni	0.000	0.002	0.000	0.000	0.000	0.000	0.005	0.000	0.001	0.004	0.001	0.003	0.000
Fe_T	0.986	1.294	1.239	2.321	1.575	1.562	1.437	1.580	1.280	1.351	1.449	1.565	0.550
Mn	0.012	0.047	0.052	0.033	0.044	0.019	0.040	0.032	0.029	0.051	0.068	0.022	0.154
Mg	0.216	1.288	0.573	0.034	0.288	0.699	0.617	0.709	0.573	1.059	1.074	0.322	0.021
Ca	1.878	0.421	1.155	0.794	1.107	0.801	0.939	0.697	1.063	0.560	0.428	1.075	2.668
Fe^{3+}													0.390
Fe^{2+}													0.160

[a] MGb, metagabbro; MGr, metagranite; MQD, metaquartz–diorite; ME, metasomatic eclogites; QFG, quartzofeldspathic gneisses; AAEA, amphibolite in amphibolite–eclogite alternations; EAEA, eclogite in amphibolite–eclogite alternations.

3.4. Amphibolite–eclogite alternations

Contrasting with the metasomatic eclogites in the Marun–Keu complex, there are also alternations of amphibolites and eclogites (see sample series PU-31 in Table 1 for mineral assemblages) with sharp contacts, which transect a penetrative banding (Fig. 4b). Both types of rocks show very similar bulk compositions, except for higher H_2O contents in the amphibolites as suggested by their higher LOI values and modal abundancies of hydrous phases (series PU-31 in Table 2). Omphacite is abundant in the eclogite, whereas in the amphibolite, it only occurs as inclusions in garnet. Rutile, which is widespread in the ec-

Table 5
Representative amphibole analyses. An extensive dataset can be found on the journal's homepage http://www.elsevier.com/locate/lithos under "Electronic Supplements"

Label	J6-7	J6-6	PU58-1	J25-2-6	PU31e2-4	PU31a-3	PU31a-4	PU-55-1	J-12-1-6	J-12-1-14	PU-34A-2	PU-34C-10
Rock-type[a]	MGb	MGb	MQD	QFG	EAEA	AAEA	AAEA	ME	ME	ME	ME	ME
Texture	Core	Rim	After Plg	Core	Core	Core	Rim	Dendritic Amp after eclogite	Amp in eclogite	Amp in amphibolite	Amp in eclogite	Amp in amphibolite
wt.%												
SiO_2	48.39	52.56	41.23	44.83	48.60	48.26	47.70	45.79	47.61	48.15	42.73	48.11
TiO_2	0.45	0.19	0.51	0.39	0.33	0.34	0.37	0.49	0.44	0.56	0.37	0.42
Al_2O_3	12.17	7.80	13.96	13.08	11.78	11.89	11.97	14.78	15.17	14.32	15.97	11.07
Cr_2O_3	0.03	0.01	0.00	0.00	0.03	0.01	0.04	0.04	0.00	0.18	0.20	0.31
NiO	0.11	0.08	0.01	0.08	0.04	0.05	0.05	0.04	0.09	0.06	0.00	0.00
FeO_T	4.71	3.63	14.88	10.85	8.39	11.73	13.19	8.84	6.78	6.88	10.92	8.63
MnO	0.00	0.04	0.08	0.03	0.04	0.14	0.17	0.08	0.09	0.17	0.05	0.06
MgO	17.03	19.20	10.89	12.60	14.08	12.49	11.17	12.78	13.99	14.39	11.46	14.72
CaO	11.03	12.23	11.35	10.98	9.21	8.91	9.76	8.80	8.97	8.30	10.52	10.23
Na_2O	2.39	1.29	2.10	2.55	3.69	3.09	2.60	4.15	3.81	4.15	3.88	3.34
K_2O	0.94	0.45	2.22	0.82	0.49	0.43	0.46	0.61	0.53	0.54	0.31	0.45
Cl	nd	nd	nd	nd	nd	nd	nd	nd	nd	nd	1.10	nd
Total	97.24	97.48	97.23	96.19	96.68	97.34	97.49	96.41	97.49	97.70	97.52	97.35
Si	6.805	7.300	6.178	6.592	6.961	6.890	6.885	6.608	6.696	6.736	6.300	6.877
Ti	0.048	0.019	0.056	0.042	0.036	0.036	0.040	0.052	0.046	0.058	0.041	0.045
Al	2.014	1.276	2.463	2.263	1.985	1.997	2.040	2.510	2.511	2.358	2.770	1.866
Cr	0.003	0.002	0.000	0.000	0.004	0.002	0.005	0.005	0.000	0.019	0.024	0.035
Ni	0.013	0.009	0.002	0.009	0.004	0.006	0.006	0.004	0.010	0.007	0.000	0.000
Fe_T	0.553	0.421	1.862	1.332	1.003	1.399	1.595	1.065	0.796	0.804	1.345	1.032
Mn	0.000	0.005	0.010	0.003	0.004	0.017	0.021	0.009	0.011	0.020	0.006	0.008
Mg	3.565	3.969	2.430	2.758	3.003	2.654	2.408	2.746	2.930	2.997	2.514	3.138
Ca	1.659	1.817	1.819	1.728	1.412	1.362	1.513	1.359	1.350	1.242	1.660	1.567
Na	0.650	0.348	0.610	0.725	1.023	0.853	0.729	1.160	1.039	1.125	1.108	0.927
K	0.168	0.079	0.423	0.153	0.089	0.079	0.085	0.113	0.095	0.097	0.059	0.081
Cl	nd	nd	nd	nd	nd	nd	nd	nd	nd	nd	0.272	nd
^{IV}Al	1.195	0.700	1.822	1.408	1.039	1.110	1.115	1.392	1.304	1.264	1.700	1.123
^{VI}Al	0.819	0.576	0.640	0.855	0.946	0.887	0.926	1.118	1.208	1.095	1.070	0.743
Fe^{3+}	0.143	0.023	0.398	0.133	0.208	0.631	0.265	0.174	0.172	0.329	0.039	0.114
Fe^{2+}	0.410	0.398	1.464	1.199	0.795	0.768	1.330	0.891	0.624	0.475	1.306	0.918
^{M4}Na	0.341	0.183	0.181	0.272	0.588	0.638	0.487	0.641	0.650	0.758	0.340	0.433
^{A}Na	0.309	0.165	0.429	0.453	0.435	0.215	0.241	0.519	0.388	0.367	0.768	0.493

nd, not determined.

[a] MGb, metagabbro; MQD, metaquartz–diorite; ME, metasomatic eclogites; QFG, quartzofeldspathic gneisses; AAEA, amphibolite in amphibolite–eclogite alternations; EAEA, eclogite in amphibolite–eclogite alternations.

logite, is mantled by sphene in the amphibolite. These evidences contrast with the ME described above and demonstrate a near-isochemical replacement of the eclogite by the amphibolite. Consequently, the boundaries between eclogites and amphibolites may represent uplift-related fluid-infiltration fronts (see Mineral Chemistry for further discussion).

4. Mineral chemistry

Mineral compositions were obtained on a Cameca Camebax electron microprobe (wavelength dispersive system) at the Mineralogical–Geological Museum (University of Oslo), using natural and synthetic mineral standards. Acceleration voltage was 15 kV and beam current was varied from 10 nA for white micas and plagioclase to 20 nA for the other phases, using defocused beam for omphacite, mica and plagioclase.

Mineral compositions are displayed in the diagrams from Figs. 5 and 6, whereas representative analyses are listed in Tables 3–6 (electronic supplements of Tables 4 and 5 are available on the journal's homepage: http://www.elsevier.com/locate/lithos).

4.1. Olivine and pyroxene

Olivine relics in metagabbros are relatively iron-rich ($\sim Fo_{75}$). Igneous and metamorphic orthopyroxene ranges in composition between En_{77} and En_{81} with low Al ($\sim 0.02–0.04$ apfu, based on 6 oxygens), whereas orthopyroxene lamellae in clinopyroxene show slightly higher Al (~ 0.08 apfu), but very similar enstatite content (En_{80}).

Igneous clinopyroxene from metagabbros is diopside with Na $\sim 0.04–0.09$ apfu (based on 6 oxygens) and low tschermakite substitution ($^{IV}Al \sim 0.02–0.06$ apfu). The composition of clinopyroxene replacing

Table 6
Representative white-mica analyses

Phase	Pheng	Pheng	Pg	Pheng	Pg	Pheng
Label	J6-10 m	J12-1-12m	J12-1-10m	J12-1-3m	J12-1-4m	J25-2-2m
Rock-type[a]	MGb	ME	ME	ME	ME	QFG
Texture	Plg pseud	Pheng in eclogite	Pg in eclogite	Pheng in amphibolite	Pg in amphibolite	Matrix
wt.%						
SiO_2	48.28	48.49	46.46	48.41	47.04	48.51
TiO_2	0.98	0.72	0.27	0.62	0.13	0.94
Al_2O_3	28.34	31.27	38.98	31.50	39.49	30.38
Cr_2O_3	0.00	0.00	0.00	0.00	0.00	0.00
NiO	0.00	0.00	0.00	0.00	0.00	0.00
FeO_T	0.76	1.45	0.53	1.30	0.62	1.88
MnO	0.01	0.00	0.00	0.01	0.00	0.00
MgO	3.65	2.44	0.22	2.74	0.20	2.39
CaO	0.08	0.03	0.45	0.00	0.43	0.04
Na_2O	0.34	1.54	7.05	2.00	7.14	0.70
K_2O	11.41	9.52	1.16	8.76	0.67	10.44
Total	93.85	95.46	95.11	95.33	95.73	95.29
Si	3.288	3.225	2.995	3.213	3.003	3.249
Ti	0.049	0.036	0.013	0.031	0.006	0.047
Al	2.272	2.448	2.958	2.461	2.967	2.395
Cr	0.000	0.000	0.000	0.000	0.000	0.000
Ni	0.000	0.000	0.000	0.000	0.000	0.000
Fe_T	0.043	0.081	0.028	0.072	0.033	0.105
Mn	0.001	0.000	0.000	0.001	0.000	0.000
Mg	0.370	0.241	0.021	0.270	0.019	0.238
Ca	0.006	0.002	0.031	0.000	0.030	0.003
Na	0.044	0.198	0.880	0.256	0.883	0.091
K	0.990	0.806	0.095	0.740	0.055	0.891

[a] MGb, metagabbro; ME, metasomatic eclogites; QFG, quartzofeldspathic gneisses.

the igneous diopside is very variable ranging from Na-rich diopside to omphacite (Na ~ 0.24–0.45 apfu). In metaquartz–diorites, clinopyroxene also presents very variable compositions, which are Na-rich diopside in plagioclase domains (Na ~ 0.29–0.36 apfu) and omphacite near garnet coronas (Na ~ 0.53 apfu) (Table 3). Cr contents in clinopyroxenes are low, but, exceptionally, omphacite surrounding Cr-spinel contains up to 3.6 wt.% Cr_2O_3.

Clinopyroxene in the more reacted rocks is omphacite with ~0.40–0.53 apfu Na and $Fe^{2+}/(Fe^{2+}+Mg)$ atomic ratios ranging from 0.09–0.21 in ME to 0.26–0.31 in QFG (Fig. 5a). The composition of clinopyroxene from the calcium-rich veins is very poor in Na with ~0.02 apfu, whereas the clinopyroxene bands at the contact between the vein and the wall rock can show up to 0.35 apfu Na (Table 3).

4.2. Garnet

In coronitic gabbros with abundant igneous relics, garnet shows large compositional variations (Fig. 5b), which depend on the composition of the domains where garnet nucleates. In plagioclase pseudomorphs and in coronas adjacent to them, garnet can be very rich in grossular (Gro_{38-60}), with moderate almandine (Alm_{32-43}) and low to very low pyrope contents (Pyr_{7-19}), whereas garnet related to orthopyroxene and olivine domains shows lower grossular contents (Gro_{14-31}), and higher pyrope (Pyr_{31-42}), but comparable almandine (Alm_{36-42}). In metaquartz–diorites, garnet composition is more homogeneous, with high almandine (Alm_{50-56}), moderate to high grossular (Gro_{26-35}) and low to moderate pyrope (Pyr_{10-16}).

The composition of garnet in metagranites is also variable depending on nucleation site (Fig. 5b). Thus, the pyrope content of garnet from the foliated matrix is low, but significant (Pyr_{8-10}), whereas in those grains growing on ilmenite, it is negligible (Pyr_1), with high almandine (Alm_{60-73}) and moderate to relatively high grossular contents (Gro_{25-37}) (Table 4).

In QFG, garnet is relatively homogeneous with high almandine (Alm_{48-51}), moderate pyrope (Pyr_{17-25}) and grossular (Gro_{25-33}) and low spessartine (Sps_{1-2}). This contrasts with more variable composition in garnet from AEA (e.g. in PU-31: Alm_{43-52}, Pyr_{19-23}, Gro_{23-36}).

In ME, garnet composition is relatively variable showing, in general, high almandine (Alm_{40-60}), moderate to high pyrope (Pyr_{25-40}) and relatively low grossular (Gro_{11-23}). However, in some eclogite–amphibolite blocks, garnet exhibits minor compositional variations, overlapping the garnet compositions from the amphibolite and the eclogite (e.g. in J-12, amphibolite: Alm_{43-50}, Pyr_{33-36}, Gro_{14-23}; eclogite: Alm_{40-50}, Pyr_{31-40}, Gro_{15-21}). In contrast, garnets from calcium-rich veins and the adjacent host rock show very large compositional differences—grossular-rich garnet (Gro_{60-97}) with variable andradite (Fe^{3+}/Fe_T atomic ratios ~ 0.07–0.70) in the vein and almandine-rich garnet in the host rock (Table 4).

4.3. Amphibole

Amphibole composition is very variable (Fig. 5c). Magnesiohornblende with significant core–rim compositional variations occurs in metagabbros (Table 5), whereas metaquartz–diorites present pargasite with ~0.18–0.25 apfu (based on 23 oxygens) ^{M4}Na, ~0.25–0.54 apfu ^{A}Na and up to 0.42 apfu of K (the highest K content found in the various rock types).

In AEA, magnesiokatophorite with relatively small compositional variations (e.g. ~0.60 apfu ^{M4}Na and ~0.42–0.44 apfu ^{A}Na (Fig. 5c)) occurs in the eclogite. This contrasts with amphibole from the adjacent amphibolite, which is barroisite in the cores and magnesiohornblende in the rims (0.21–0.64 apfu ^{M4}Na (Fig. 5c)). High *P* experiments indicate that ^{M4}Na buffered by garnet and plagioclase tends to increase with pressure (Poli, 1993). Therefore, the significant ^{M4}Na decrease towards the grain rims detected in amphibole from the amphibolite (Table 5) may indicate decompression during the replacement of eclogites by amphibolitic assemblages.

Compared to the eclogites previously described, amphibole in QFG, which coexists with omphacite and plagioclase, presents rather similar ^{A}Na contents (~0.45–0.49 apfu), but significantly lower ^{M4}Na (~0.27 apfu) (Fig. 5c).

In metasomatic blocks, the amphibole from both eclogite and amphibolite bands can be barroisite with very close compositions (see series J-12 in Table 5), which are also similar to those of dendritic amphiboles replacing eclogitic assemblages (Table 5). How-

ever, in other blocks (e.g. see series PU-34 in Table 5), amphibole composition is more variable ranging from pargasite and edenite in the eclogite to magnesiotarramite and magnesiokatophorite in the amphibolite. In veins with Cl–apatite, amphibole can contain up to 0.27 apfu Cl.

4.4. White mica

White mica is typically phengite with 3.19–3.36 apfu Si (based on 11 oxygens) (Table 6). Coexisting paragonite and phengite in the ME (J-12 in Table 6) show K/(Na+K) atomic ratios of 0.06–0.10 and 0.61–0.82, respectively. In QFG, phengite displays also high Na contents (~0.85–0.89 K/(Na+K) atomic ratios), whereas phengite in metagabbros is poor in Na with K/(Na+K) atomic ratios ~0.96.

The compositional variations shown by the white micas are consistent with the semiquantitative phengite-corrected paragonite–muscovite solvus by Guidotti et al. (1994) for $T \sim 500–600$ °C and moderate pressures (Fig. 6). This semiquantitative solvus shows a compositional shift of phengite towards the muscovite end-member at $P > 15$ kbar. Therefore, the relatively low K/(Na+K) atomic ratios in phengite coexisting with paragonite suggest $P < 15–16$ kbar for the eclogite-facies metamorphism, which is consistent with the stability of plagioclase in the more felsic rocks types (see below).

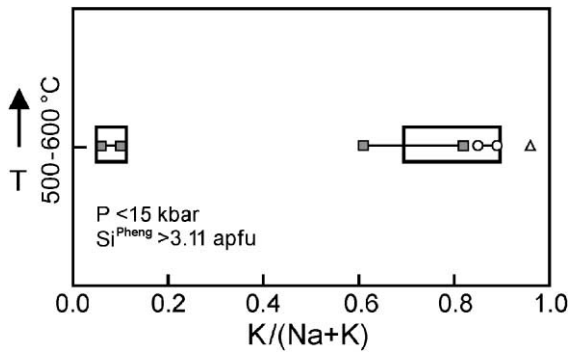

Fig. 6. White mica composition in the rocks from the Marun–Keu complex. Symbols as in Fig. 5, except grey squares, coexisting paragonite and phengite in the metasomatic eclogite J-12. Boxes indicate the compositional range of coexisting paragonite and phengite at temperatures between 500 and 600 °C for paragonite–phengite pairs formed at $P < 15$ kbar with $Si^{Pheng} > 3.11$ apfu (Fig. 2 in Guidotti et al., 1994).

4.5. Epidote-group minerals

Coronitic gabbros present zoisite/clinozoisite with low pistacite contents ($Fe_2O_3 < 2$ wt.%), whereas clinozoisite with higher pistacite contents occurs in ME (5–6 wt.% Fe_2O_3) and in QFG (3–7.5 wt.% Fe_2O_3).

4.6. Plagioclase

Plagioclase in the quartzofeldspathic rocks is oligoclase (Ab_{84-87}) with negligible K, whereas in amphibolites from AEA is very close to the albite end-member component.

5. *P–T* conditions during the eclogite-facies metamorphism of the Marun–Keu complex

Temperatures for the eclogite-facies event were estimated using various calibrations of the garnet–clinopyroxene thermometer (Ellis and Green, 1979; Krogh, 1988; Ai, 1994; Krogh-Ravna, 2000). In addition, temperatures were also computed by nonlinear mineral-equilibrium calculations (as described in Molina and Poli, 2000) using the end-member reaction:

3 diopside + almandine = 3 hedenbergite + pyrope.

The calculations were performed using the thermodynamic database of Holland and Powell (1990) (revised 1994), with the solution models for garnet by Berman (1990) and for clinopyroxene by Holland (1990).

The calculated temperatures for rim compositions of adjacent grains of garnet and clinopyroxene in rock-matrix and vein assemblages are listed in Table 7. Before evaluating the temperature conditions during the eclogite-facies metamorphism, it is necessary to perform an assessment of the accuracy of the different thermometric methods.

Temperatures given by the calibration of Krogh-Ravna (2000) are very close to those of the Ai (1994) thermometer, whereas the calibrations of Ellis and Green (1979) and Krogh (1988) give systematically higher values. Notably, temperatures obtained for ME by nonlinear mineral-equilibrium calculations and with the calibration of Krogh-Ravna (2000) are almost identical.

Table 7
Temperature estimates

Garnet–clinopyroxene thermometer[a]													
Label	PU34D-1	PU34D-2	PU34D-3	J12-1-1	J12-1-2	J12-1-3	J25-2-3	J25-4-5	J25-9-10	J25-12-13	J6-1	J6-4	J6-8
Rock type[b]	ME	ME	ME	ME	ME	ME	QFG	QFG	QFG	QFG	MGb	MGb	MGb
$Kd^{Gar/Cpx}_{Fe/Mg}$	12.8	9.22	8.01	11.2	7.15	7.12	8.24	7.25	8.17	7.42	7.50	7.40	7.07
Gro	0.15	0.16	0.17	0.19	0.17	0.19	0.27	0.28	0.26	0.27	0.23	0.22	0.22
$Mg/(Mg+Fe)^{Gar}$	0.34	0.37	0.35	0.44	0.44	0.42	0.29	0.31	0.31	0.31	0.51	0.52	0.53
T (°C) at 10 kbar													
Ai(94)	406	476	526	448	527	561	621	660	607	643	558	550	567
K(88)	484	566	615	558	633	673	720	763	708	745	696	688	710
EG(79)	539	610	650	592	670	695	721	758	712	743	706	702	720
KR(00)	437	506	552	475	552	585	630	667	618	648	569	564	577
MEC[c]	436± 60	504± 59	560± 66	472± 58	580± 68	595± 68	586± 65	622± 68	585± 66	614± 68	620± 68	598± 67	637± 70
T (°C) at 15 kbar													
Ai(94)	430	503	554	474	556	590	649	689	635	672	586	579	596
K(88)	512	596	647	587	665	706	752	796	740	778	728	720	743
EG(79)	550	624	664	604	684	709	735	772	725	757	720	716	734
KR(00)	460	531	578	498	579	612	656	694	643	674	595	590	604
MEC[c]	460± 60	530± 60	584± 67	494± 58	607± 69	622± 69	612± 66	650± 69	610± 66	641± 68	647± 69	624± 67	664± 70
T (°C) at 20 kbar													
Ai(94)	455	530	582	499	585	620	677	718	663	700	615	607	625
K(88)	540	627	678	615	698	738	783	828	771	810	760	753	776
EG(79)	563	637	678	617	699	723	748	786	739	771	734	730	748
KR(00)	482	555	604	521	605	638	681	720	669	700	622	616	630
MEC[c]	487± 60	553± 60	610± 68	516± 59	633± 70	650± 70	638± 66	677± 70	637± 67	668± 69	674± 69	650± 68	692± 71

[a] Ai(94), Ai (1994); EG(79), Ellis and Green (1979); K(88), Krogh (1988); KR(00), Krogh-Ravna (2000); MEC, mineral-equilibrium calculations.

[b] ME, metasomatic eclogites; MGb, metagabbro; QFG, quartzofeldspathic gneisses.

[c] Error on temperature estimates propagated from uncertainties in enthalpy of formation of minerals reported by Holland and Powell (1990), in pressure (relative error ~ 5%) and in mineral compositions (relative errors ~ 1–2.5%), using the Monte Carlo method (Anderson, 1976) (number of iterations = 100).

Whatever the thermometric method, the scattering of the calculated T (at constant P) is minor or negligible in QFG and in metagabbros (<60 °C), whereas in ME, it is very large (>150 °C). Since variations in mineral compositions are minor within each group (Table 7), the large T range in ME may be significant and may reflect specific processes experienced by this type of rocks (we are preparing a work for further discussion). In contrast, comparing T_{max} in the different rock types, nonlinear mineral-equilibrium calculations give the smallest dispersion with a T range of ca. 40 °C, which contrasts with larger T_{max} differences (63–100 °C) with the various thermometer calibrations. Since the garnets of the different rock types present significant compositional differences (Table 7), the larger scattering in T_{max} given by the thermometers may reveal a deficient correction for compositional dependences of the Fe–Mg fractionation between garnet and clinopyroxene.

Therefore, T estimates obtained by nonlinear mineral-equilibrium calculations, which seem to give more accurate results, were preferred in this study.

According to this method, it is likely that the T_{max} registered by the central and southern parts of the Marun–Keu complex during the eclogite-facies metamorphism could be of ca. 600–650 °C at 15 kbar. These values are consistent with H_2O-saturated stability phase fields of paragonite and phengite (Franz and Althaus, 1977; Schmidt and Poli, 1998) (Fig. 7) and with temperature estimates given by Udovkina (1971), which are significantly lower than those reported by Dobretsov and Sobolev (1984) and Sobolev et al. (1986) (Table 9).

Pressures for the eclogite-facies stage were estimated using the garnet–clinopyroxene–phengite barometer of Waters and Martin (1993). Additionally, pressure calculations were also performed in QFG with the subassemblage plagioclase + omphacite + quartz by mineral-equilibrium calculations as previously described through the end-member reaction:

albite = jadeite + quartz,

employing the solution models for clinopyroxene by Holland (1990) and for plagioclase by Furhman and Lindsley (1988). The *P* estimates for rim compositions of adjacent grains in rock-matrix assemblages are listed in Table 8. *P* values range from 15 kbar at 700 °C to 18 kbar at 550 °C with the garnet–clinopyroxene–phengite barometer, and from 12 kbar at 550 °C to 15 kbar at 700 °C with the mineral-equilibrium calculations. These *P* estimates are consistent with the stability of paragonite, which breaks down at high pressures by the reaction (Holland, 1979):

paragonite = kyanite + jadeite + H_2O.

The calculated pressures are close to those reported by Dobretsov and Sobolev (1984) for blueschist assemblages from the northern part of the Marun–Keu complex and by Schulte and Blümel (1999) for eclogites from the Maksyutov complex (Southern Urals) (Table 9). This implies similar depths for the low *T* and medium *T* eclogite-facies metamorphism of the Marun–Keu complex. Therefore, the central and southern parts of this complex could represent a crustal domain with a warm, disturbed geotherm (a further discussion follows in our work in preparation).

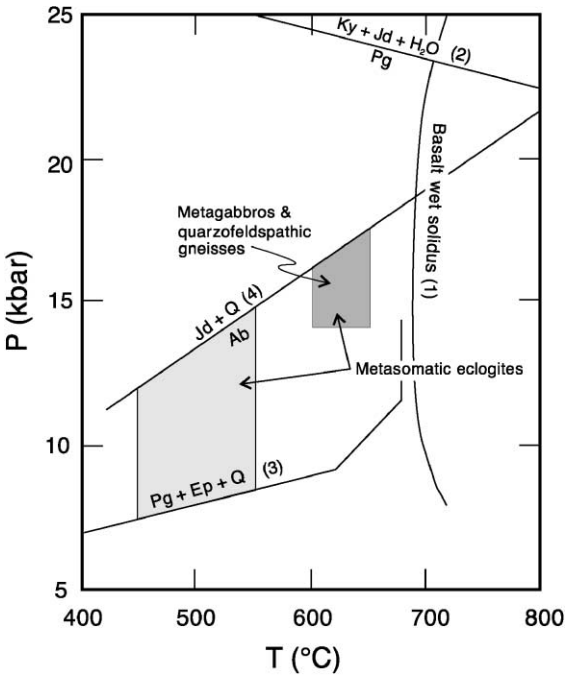

Fig. 7. Pressure–temperature conditions for the eclogite-facies metamorphism in the central and southern parts of the Marun–Keu complex, with experimentally determined reactions of relevance to define the stability field of the high P rocks. Grey areas are *P–T* conditions consistent with nonlinear mineral-equilibrium calculations and with the stability of Na-rich plagioclase during the high*P*metamorphism. Note poor pressure constraints for the lower temperature estimates in the metasomatic eclogites. (1) Basalt wet solidus from Schmidt and Poli (1998); (2) Holland (1979); (3) Franz and Althaus (1977); (4) Holland (1980).

6. Discussion

6.1. Importance of fluids during eclogitization in the Marun–Keu complex

The presence of fluids and ductile deformation (which, in turn, may be a consequence of weakening by fluid-catalyzed reactions) have been considered as the most important factors able to overcome the kinetic barriers preventing eclogitization (e.g. Wayte et al., 1989; Rubie, 1990; Austrheim et al., 1997).

In metagabbros from the Marun–Keu complex, the importance of fluids for the process of eclogitization can be inferred from the presence of partially reacted domains with disequilibrium reaction textures. In these rocks, the occurrence of mineral transformations along microveins and grain boundaries as well as the

Table 8
Pressure estimates

Garnet–clinopyroxene–phengite barometer-WM(93)[a]			Albite–jadeite–quartz barometer–MEC[a,b]			
Label	J-12-1	J-25-2	Label	J-25-2	J-25-2	J-25-2
Rock type[c]	ME	QFG	Rock type[c]	QFG	QFG	QFG
$Kd_{Fe/Mg}^{Gar/Cpx}$	7.15	8.17	Ab	0.84	0.84	0.84
Gro	0.17	0.26	Jd	0.41	0.42	0.43
Si^{pheng}	3.23	3.25				
$K/(Na+K)^{Pheng}$	0.80	0.91				
T (°C)	*P (kbar)*	*P (kbar)*	*T (°C)*	*P (kbar)*	*P (kbar)*	*P (kbar)*
550	18±2	17±2	550	12±3	13±2	13±2
600	17±2	17±2	600	13±3	13±2	13±2
650	16±1	16±2	650	14±3	14±2	14±2
700	15±2	16±2	700	15±3	14±2	15±2

[a] WM(93), Waters and Martin (1993); MEC, mineral-equilibrium calculations.
[b] Error on pressure estimates propagated from uncertainties in enthalpy of formation of minerals reported by Holland and Powell (1990), in temperature (relative error ~ 5%) and in mineral compositions (relative errors ~ 1–2.5%), using the Monte Carlo method (Anderson, 1976) (number of iterations = 100).
[c] ME, metasomatic eclogites; QFG, quartzofeldspathic gneisses.

Table 9
Summary of *P–T* conditions and ages for the eclogite-facies stage in various metamorphic complexes along the Urals[a]

Complex	Type of eclogite	*P–T* conditions	Age	Locality
Marun–Keu	medium-*T* eclogites and low *T* eclogites	450–650 °C and 14–17 kbar (1) (Middle and Southern parts) 550–900 °C and 8–16 kbar (2) 600 °C and 14 kbar (3) 500°C and 10–11 kbar (4) (Northern part) 700 °C and 12 kbar (4) (Middle and Southern parts)	358±3 Ma (5)	Polar Urals
Voikar	low *T* eclogites (2)			Polar Urals
Kharuta–Pe	low *T* eclogites (2)			Polar Urals
Salatim	low *T* eclogites (2)			Middle Urals
Maksyutov	low *T* eclogites	550–600 °C and >15 kbar (2) 620±70 °C and >15 kbar (6) >27 kbar (coesite pseudomorphs?, 7) >32 kbar (diamond pseudomorphs?, 6, 8) 550–600 °C and 25 kbar (10) 600 °C and > 15 kbar (11) 480–500 °C at 11 kbar to 530–600 °C at 15 kbar (12) 543–603 °C and 17 kbar (13) 468–516 °C and 16 kbar (13) <25 kbar (14)	prior to 370–380 Ma (6) 380 Ma (9) 375±2 Ma (14)	South Urals
Khabarny	low *T* eclogites (2)			South Urals

[a] Refs.: (1) this work; (2) Sobolev et al. (1986); (3) Udovkina (1971); (4) Dobretsov and Sobolev (1984); (5) Glodny et al. (1999); (6) Lennykh et al. (1995); (7) Chesnokov and Popov (1965); (8) Leech and Ernst (1998); (9) Matte et al. (1993); (10) Dobretsov (1991); (11) Beane et al. (1995); (12) Schulte and Blümel (1999); (13) Hetzel et al. (1998); (14) Glodny et al. (in press).

growth of eclogitic hydrous phases indicate that mass transport across the rock matrix was enhanced by H_2O-dominated fluids. Eclogitization of dry rocks along microveins was firstly reported by Austrheim (1987) and by Erambert and Austrheim (1993) in granulites from Bergen Arcs, stressing the importance of fluid infiltration rather than intracrystalline diffusion as the mass-transport mechanism at relatively low temperatures (e.g. $T<700$ °C).

In the case of QFG and of ME, the reaction histories are more difficult to decipher because the transformations to eclogite-facies assemblages have gone to completion. In both cases, it may be impossible to estimate the bulk H_2O contents before eclogitization, which is a key point to understanding the reaction mechanisms as discussed before. If hydrous phases were present in the protoliths, eclogitization could have progressed by dehydration reactions as suggested by results of H_2O-saturated experiments (e.g. Poli and Schmidt, 1995; Schmidt and Poli, 1998). This means that kinetic barriers could be overcome by internal H_2O production, and an almost continuous transformation should be expected if H_2O was available. On the contrary, if the amount of hydrous phases was insufficient to saturate the rock pores with H_2O from dehydration reactions, eclogitization could be a discontinuous process, occurring only under more advantageous conditions (e.g. mass-transport enhanced by deformation or H_2O external supply) rather than at the T_{max} experienced by the metamorphic complex (see Engvik et al. (2000) for further discussions). Accordingly, the large temperature variations in rim assemblages from ME may be a consequence of a complex fluid-circulation history through the fracture networks.

6.2. Metasomatism during eclogitization: implications for $P-T$ evolution of the Marun–Keu complex

The growth of eclogite rinds after amphibolites and poikiloblastic amphibole replacing omphacite–garnet assemblages are two of the most striking features of the metasomatism experienced by the Marun–Keu complex. It is important to point out that if metasomatism was not taken into account, a complicated metamorphic $P-T$ evolution for the Marun–Keu complex should be inferred, with amphibolite-facies events before and after the eclogite-facies metamorphism.

In the previous sections, it has been argued for the formation of these assemblages during the eclogite-facies metamorphism. Below, mass-balance calculations have been performed to evaluate whether these transformations were isochemical or not. Mass balances between omphacite, garnet, amphibole and quartz were performed by least-square methods (Table 10),

Table 10
Mass-balance calculations in metasomatic assemblages in the system NCFMAS[a]

Label[b]	J-12	PU-55
Phase relations	Amphibolite replaced by eclogite	Eclogite replaced by dendritic amphibole
Reaction coefficients (wt)[c]		
Gar	0.273	−0.339
Cpx	0.727	−0.661
Amp	−0.961	0.957
Q	−0.039	0.043
Mass differences for total mass in NCFMAS=100 (in weigth)		
SiO_2	−0.72	0.28
Al_2O_3	−0.39	−0.18
FeO_T	1.71	0.93
MgO	−5.37	4.16
CaO	4.01	−3.20
Na_2O	0.68	−0.001

[a] H_2O and K_2O considered as perfectly mobile components, i.e. any unbalance in these components is accounted by the external medium.
[b] Calculations performed employing mineral compositions from Tables 3, 4 and 5, assuming conservation of the total mass.
[c] Positive reaction coefficients for the product assemblage.

assuming conservation of the total mass in the system SiO_2, Al_2O_3, FeO_T, MgO, CaO and Na_2O, i.e. H_2O and K_2O are considered as perfectly mobile components. The results give significant unbalances in MgO and CaO with absolute mass differences > 2 (in weight referred to a total mass = 100) in the two cases (Table 10). Therefore, these calculations evidence that the discussed mineral replacements cannot be isochemical. In addition, since mineral compositions in the considered transformations are similar, product components during the growth of the omphacite rim (mostly MgO) become reactant components during the growth of the dendritic amphibole for the considered reference frame. This contrasting behaviour could be caused by differences in local factors such as fluid or initial rock compositions, hydrodynamics of the fracture fluids, or mass-transport mechanisms across the matrix rocks, rather than differences in the $P–T$ conditions — although these cannot be disregarded — since both replacements occurred during the eclogite-facies metamorphism.

6.3. Metasomatic blocks: protoliths and nature of the infiltrating fluids

Since a large variety of metasomatic sequences exists in the Marun–Keu complex, their protoliths could be very heterogeneous and a systematic analysis of the various metasomatic rocks should be done to constrain the protolith nature(s). Even though this is beyond the scope of this work, below we discuss the compositional variations across a phengite-bearing metasomatic block (sample J-12), which is one of the most widespread metasomatic rock types. In order to gain insights into the nature of its protolith, the composition of the different metasomatic bands in block J-12 (Table 1) is compared to that of metagabbros, metagranites and metaquartz–diorites in the Primitive Mantle-(PM) normalized diagram from Fig. 8. It is interesting to note that in the vein infilling, which presents abundant omphacite and phengite, the contents in Rb, U, Th K, Sr, Zr, FeO and Cr are comparable to those in metagranites and in metaquartz–diorites, whereas Pb, Y, V, CaO, MgO and Ni contents lie within the compositional range defined by metagabbros (Fig. 8). Compared to the vein infillings, the eclogite rind and the amphibolite core present lower Rb, U, Th, K, Nb, Sr, Zr, V and TiO_2 and higher Y, FeO, Cr and Co, with the PM-normalized pattern for most analyzed chemical components of the eclogite rind lying in between those of the vein infilling and the amphibolite core (Fig. 8). These geochemical features evidence an increase in the signature of the "granite component" towards the

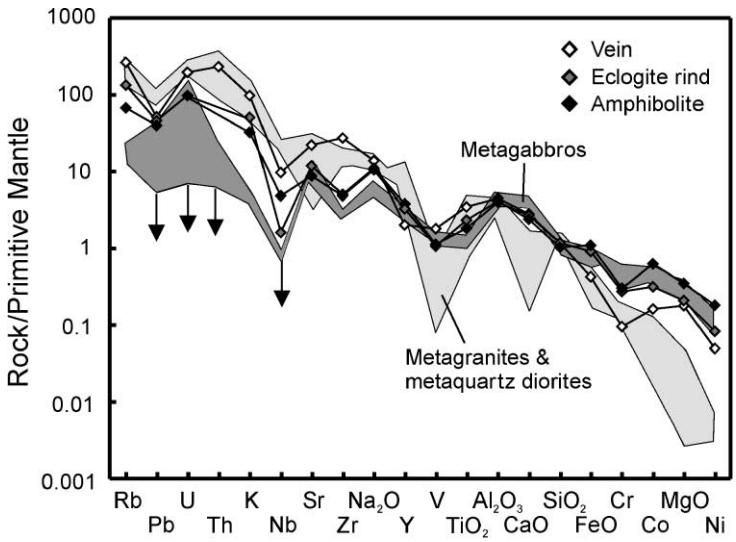

Fig. 8. Whole-rock Primitive Mantle-normalized major and trace elements from Marun–Keu rocks. Normalization values after Hofmann (1988), except V and Cr which are after McDonough and Sun (1995).

vein. Although the origin of the fracture fluids cannot be determined with the present data, these geochemical relations suggest the interaction of externally derived, silica-alkali-rich fluids with mafic rocks, leading to the replacement of amphibole-rich assemblages by omphacite.

However, the geochemical data from sample J-12 (Fig. 8) also provide evidence that may support the formation of the amphibolite during the metasomatic process. The amphibolite presents MgO, Co and Ni contents close to the maximum contents shown by metagabbros, whereas K and Rb are significantly higher than in metagabbros (Fig. 8). Therefore, if the protolith of the amphibolite was a gabbro similar to those from Mica Mountain (e.g. samples PU-62 and PU-63C in Table 2), the core of the block should also have experienced substantial metasomatism and recrystallization during the eclogite-facies metamorphism. This implies that the amphibolite core may not be a relic assemblage of an early metamorphism, but that both amphibolite and eclogite formed at the same time. This is supported by Rb/Sr mineral data for the amphibolite and the eclogite of sample J-12, which suggest Sr-isotopic equilibrium between these lithotypes, and define a common isochron age of 358±3 Ma (Glodny et al., 1999, in preparation) (Table 9).

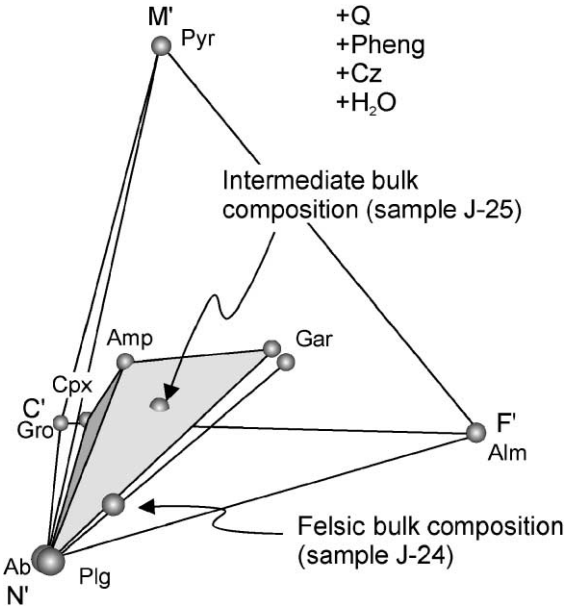

Fig. 9. Phase relations in the system $Na_2O-K_2O-CaO-FeO+MnO-MgO-Al_2O_3+F_2O_3-SiO_2-H_2O$ (NKCFMASH) of high *P* mineral assemblages in QFG displayed in the N′ C′ F′ M′ chemography projected from quartz, phengite and clinozoisite, considering H_2O as a perfectly mobile component. In this projection, the transformed coordinates N′, C′, F′ and M′ were selected to coincide, respectively, with the plotting position of albite, grossular, almandine and pyrope.

6.4. Chemographic relationships in the QFG: compositional factors controlling the occurrence of omphacite

Textural relations evidence that oligoclase and omphacite may coexist in QFG during the eclogite-facies metamorphism. Indeed, oligoclase–omphacite assemblages are widespread in high *P* granulite-facies terrains as in the Sudetes, SW Poland (e.g. Smulikowski, 1967; Smulikowski and Bakun-Czubarow, 1973; Pouba et al., 1985; Bakun-Czubarow, 1991; Kryza et al., 1996).

In the previous sections, it was mentioned that the fine-scale layering of omphacite-free and omphacite-bearing assemblages in the felsic rock could be controlled by the bulk chemistry. To assess this possibility, the mineral assemblages from the QFG with felsic and intermediate compositions are displayed in the chemographic projection of Fig. 9. In agreement with a compositional control, the felsic composition (sample J-24) plots along the garnet–plagioclase tie-line, whereas the intermediate composition (sample J-25) lies in the garnet–clinopyroxene–amphibole–plagioclase tetrahedron (Fig. 9). This chemography also suggests that an impoverishment in the N′ component may cause the disappearance of plagioclase from the garnet–clinopyroxene–amphibole–plagioclase assemblage. This is consistent with experimental evidences which suggest that plagioclase may be stable at eclogite-facies conditions in relatively felsic rocks such as meta-anorthosites and meta-andesites, whereas in mafic systems it may be absent (e.g. Ringwood, 1975 and references therein; see also Carswell, 1990).

7. Conclusions

In the Marun–Keu complex, Neoproterozoic-to-Cambrian volcanic-sedimentary sequences with abundant intrusive mafic to felsic rocks, experienced late

Devonian to early Carboniferous metamorphism at eclogite-facies conditions. T_{max} of ca. 600–650 °C and P ranging 14–17 kbar are recorded in the central and southern parts of the complex.

Nondeformed, dry intrusive rocks remain unreacted during metamorphism, preserving their igneous mineralogy, whereas transformation into eclogite-facies assemblages can run to completion in sheared bands and in domains infiltrated by H_2O-dominated fluids. Eclogitization of dry rocks is a discontinuous process controlled by fluid availability or deformation.

Infiltration of silica–alkali-rich fluids, out of equilibrium with the host-rock, caused metasomatism in the Marun–Keu complex during the eclogite-facies metamorphism, growing a large variety of mineral band sequences.

Eclogite-facies metasomatism produced complex eclogite–amphibolite replacements, which may lead to construction of complicated and erroneous $P–T$ orogenic evolutions if the mass redistribution involved in these transformations is not considered or overlooked.

Acknowledgements

We thank M. Erambert, W.H. Peck and S. Poli for their constructive commenlts and corrections. We are indebted to V. Koroteev, V.I. Lennykh and V. Pease for excellent guidance and company in the field. The thorough and constructive reviews by M. Scambelluri and P.J. O'Brien are greatly appreciated. Field work in the Polar Urals was made possible through a grant from the Nansen Foundation to H. Austrheim. This work was funded by grants from the European Commission (TMR-URO Programme, contract No. ERBFMRXCT96-0009). The work was completed during J.F. Molina's stay at the Dipartimento di Scienze della Terra of Milan University (contract DR 198199-30/03/00 S. Poli).

References

Ahrens, T.J., Schubert, G., 1975. Gabbro–eclogite reaction rates and its geophysical significance. Rev. Geophys. Space Phys. 13, 383–400.

Ai, Y., 1994. A revision of the garnet–clinopyroxene Fe^{2+}–Mg exchange geothermometer. Contrib. Mineral. Petrol. 115, 467–473.

Anderson, G.M., 1976. Error propagation by the Monte Carlo method in geochemical calculations. Geochim. Cosmochim. Acta 40, 1533–1538.

Austrheim, H., 1987. Eclogitization of the lower crustal granulites by fluid migration through shear zones. Earth Planet. Sci. Lett. 81, 221–232.

Austrheim, H., 1998. Influence of fluids and deformation on metamorphism of the deep crust and consequences for the geodynamics of collision zones. In: Hacker, B.R., Liou, J.G. (Eds.), Geodynamics and Geochemistry of Ultrahigh-Pressure Rocks. Kluwer Academic Publishing, Netherlands, pp. 297–323.

Austrheim, H., Erambert, M., Engvik, A.K., 1997. Processing of crust in the root of the Caledonian continental collision zone: the role of eclogitization. Tectonophysics 273, 129–153.

Bakun-Czubarow, N., 1991. Geodynamic significance of the Variscan high-P eclogite–granulite series of the Zlote Mountains in the Sudetes. Pub. Geoph. Polish Acad. Sci., A 19 (236), 215–244.

Bea, F., Fershtater, G., Montero, P., Smirnov, V., Zin'kova, E., 1997. Generation and evolution of subduction-related batholiths from the central Urals: constraints on the $P–T$ evolution history of the Uralian orogen. Tectonophysics 276, 103–116.

Beane, R.J., Liou, J.G., Coleman, R.G., Leech, M.L., 1995. Petrology and retrograde $P–T$ path for eclogites of the Maksyutov complex, Southern Ural Mountains, Russia. Isl. Arc. 4, 254–266.

Bebout, G., Barton, M.D., 1993. Metasomatism during subduction: products and possible paths in the Catalina Schist, California. Chem. Geol. 108, 61–92.

Berman, R.G., 1990. Mixing properties of Ca–Mg–Fe–Mn garnets. Am. Mineral. 75, 328–344.

Bezzubtsev, V., Zalyaleev, R., Sakovich, A., 1986. Geological map of the Gorny Taimyr 1:500,000 — Explanatory Note, Krasnoyarsk, 177 pp. (in Russian).

Biino, G., Compagnoni, R., 1992. Very high-pressure metamorphism of the Brossasco coronitic metagranite, southern Dora Maira massif, Western Alps. SMPM 72, 347–363.

Brown, D., Juhlin, C., Alvarez-Marron, J., Perez-Estaun, A., Oslianski, A., 1998. Crustal-scale structure and evolution of an arc-continent collision zone in the southern Urals, Russia. Tectonics 17, 158–171.

Carswell, D.A., 1990. Eclogites and eclogite facies: definitions and classifications. In: Carswell, D.A. (Ed.), Eclogite Facies Rocks. Blackie, Glasgow, pp. 1–13.

Chesnokov, B.V., Popov, V.A., 1965. Increasing volume of quartz grains in eclogites of the South Urals. Dokl. Akad. Nauk 62, 909–910 (in Russian).

Compagnoni, R., Maffeo, B., 1973. Jadeite-bearing metagranites l.s. and related rocks in the Mount Mucrone area (Sesia Lanzo zone, Western Italian Alps). SMPM 53, 355–378.

Compagnoni, R., Dal Piaz, G.V., Hunziker, J.C., Gosso, G., Lombardo, B., Williams, P.F., 1977. The Sesia Lanzo zone, a slice of continental crust with alpine high-pressure/low-temperature assemblages in the western Italian Alps. Rend. Soc. Ital. Mineral. Petrol. 33, 281–334.

Dobretsov, N.L., 1991. Blueschists and eclogites: a possible plate

tectonic mechanism for the emplacement from the upper mantle. Tectonophysics 186, 253–268.

Dobretsov, N.L., Sobolev, N.V., 1970. Eclogites from metamorphic complexes of the USSR. Phys. Earth Planet. Inter. 3, 462–470.

Dobretsov, N.L., Sobolev, N.V., 1984. Glaucophane schists and eclogites in folded systems from Northern Asia. Ofioliti 9, 401–424.

Ellis, D.J., Green, D.H., 1979. An experimental study of the effect of Ca upon garnet–clinopyroxene Fe–Mg exchange equilibria. Contrib. Mineral. Petrol. 71, 13–22.

Engvik, A.K., Austrheim, H., Andersen, T.B., 2000. Structural, mineralogical and petrophysical effects on deep crustal rocks of fluid-limited polymetamorphism, Western Gneiss Region, Norway. J. Geol. Soc. (London) 157, 121–134.

Erambert, M., Austrheim, H., 1993. The effect of fluid and deformation on zoning and inclusion patterns in polymetamorphic garnets. Contrib. Mineral. Petrol. 115, 204–214.

Ernst, W.G., Liou, J.G., Coleman, R.G., 1995. Comparative petrotectonic study of five Eurasian ultra-high pressure metamorphic complexes. Int. Geol. Rev. 37, 191–211.

Fershtater, G.B., Montero, P., Borodina, N.S., Pushkarev, E.V., Smirnov, V.N., Bea, F., 1997. Uralian magmatism: an overview. Tectonophysics 276, 87–102.

Franz, G., Althaus, E., 1977. The stability relations of the paragenesis paragonite–zoisite–quartz. N. J. Min. Abh. 130, 159–167.

Furhman, M.L., Lindsley, D.H., 1988. Ternary-feldspar modelling in thermobarometry. Am. Mineral. 37, 201–215.

Gil-Ibarguchi, J.I., Mendia, M., Girardeau, J., 1991. Mg-rich and Cr-rich staurolite and Cr-rich kyanite in high-pressure ultrabasitic rocks (Cabo Ortegal, North-western Spain). Am. Mineral. 76, 501–551.

Gilotti, J.A., Elvevold, S., 1998. Partial eclogitization of the Ambolten gabbro–norite, North–east Greenland Caledonides. SMPM 78, 273–292.

Glodny, J., Austrheim, H., Montero, P., Rusin, A., 1999. The Marun–Keu metamorphic complex, Polar Urals, Russia: Protolith ages, eclogite-facies fluid–rock interaction, and exhumation history. EUG 10, Strasbourg, France, 80.

Glodny, J., Austrheim, H., Rusin, A., 2000. Dating of subduction-related fluid mineralizations: constraints on the life span of a Paleozoic subduction system in the Polar Urals, Russia. Goldschmidt 2000. Oxford, UK. J. Conf. Abstr. 5, 446.

Glodny, J., Pease, V.L., Montero, P., Austrheim, H., Rusin, A., in preparation. Protolith ages of eclogites, Marun–Keu complex, Polar Urals, Russia: Implications for the pre- and early Uralian evolution of the NE European continental margin.

Glodny, J., Bingen, B., Austrheim, H., Molina, J.F., Rusin, A., in press. Precise eclogitization ages deduced from Sr/Rb mineral systematics: The Maksyutov complex, Southern Urals, Russia. Geochim. Cosmochim. Acta.

Gómez-Pugnaire, M.T., Karsten, L., López-Sánchez-Vizcaíno, V., 1997. Phase relationships and $P–T$ conditions of coexisting eclogite–blueschists and their transformation to greenschist-facies rocks in the Nerkau Complex (Northern Urals). Tectonophysics 276, 195–216.

Guidotti, C.V., Sassi, F.P., Blencoe, J.G., 1994. The effects of ferromagnesian components on the paragonite–muscovite solvus: a semiquantitative analysis based on chemical data for natural paragonite–muscovite pairs. J. Metamorph. Geol. 12, 779–788.

Hetzel, R., Echtler, H.P., Seifert, W., Schulte, B.A., Ivanov, K.S., 1998. Subduction- and exhumation-related fabrics in the Paleozoic high-pressure, low-temperature Maksyutov complex, Antigan area, southern Urals, Russia. GSA Bull. 110, 916–930.

Hofmann, A.W., 1988. Chemical differentiation of the Earth: the relationship between mantle, continental crust, and oceanic crust. Earth Planet. Sci. Lett. 90, 297–314.

Holland, T.J.B., 1979. Experimental determination of the reaction paragonite = jadeite + kyanite + quartz + H_2O and internally consistent thermodynamic data for part of the system Na_2O–Al_2O_3–SiO_2–H_2O with application to eclogites and blueschists. Contrib. Mineral. Petrol. 68, 293–301.

Holland, T.J.B., 1980. The reaction albite = jadeite + quartz determined experimentally in the range 600–1200 °C. Am. Mineral. 65, 129–134.

Holland, T.J.B., 1990. Activities of components in omphacitic solid solution. An application of Landau theory to mixtures. Contrib. Mineral. Petrol. 105, 446–453.

Holland, T.J.B., Powell, R., 1990. An enlarged and updated internally consistent thermodynamic data set with uncertainties and correlations: the system K_2O–Na_2O–CaO–MgO–MnO–FeO–Fe_2O_3–Al_2O_3–TiO_2–SiO_2–C–H_2–O_2. J. Metamorph. Geol. 8, 89–124.

Jamtveit, B., Austrheim, H., Malthe-Sorenssen, A., 2000. Accelerated hydration of the Earth's deep crust induced by stress perturbations. Nature 408, 75–78.

Koons, P.O., Rubie, D.C., Frueh-Green, G., 1987. The effects of disequilibrium and deformation on the mineralogical evolution of quartz diorite during metamorphism in the eclogite facies. J. Petrol. 28, 679–700.

Krogh, E.J., 1988. The garnet–clinopyroxene Fe–Mg geothermometer — a reinterpretation of existing experimental data. Contrib. Mineral. Petrol. 99, 44–48.

Krogh-Ravna, E., 2000. The garnet–clinopyroxene Fe^{2+}–Mg geothermometer: an updated calibration. J. Metamorph. Geol. 18, 211–219.

Kryza, R., Pin, C., Vielzeuf, D., 1996. High-pressure granulites from the Sudetes (south-west Poland): evidence of crustal subduction and collisional thickening in the Variscan Belt. J. Metamorph. Geol. 14, 531–546.

Leech, M., Ernst, W.G., 1998. Graphite pseudomorphs after diamond? A carbon isotope and spectroscopic study of graphite cuboids from the Maksyutov complex, south Ural Mountains, Russia. Geochim. Cosmochim. Acta 62, 2143–2154.

Lennykh, V.I., Valizer, P.M., Beane, R.J., Leech, M.L., Ernst, W.G., 1995. Petrotectonic evolution of the Maksyutov complex, southern Urals, Russia: implications for ultrahigh-pressure metamorphism. Int. Geol. Rev. 37, 584–600.

Lennykh, V.I., Valizer, P., Schulte, B.A., 1997. Eclogites and blueschists of the Urals: evolution and geodynamics. Terra Nova 9, 17.

Manning, C.E., 1998. Fluid composition at the blueschist–eclogite transition in the model system Na_2O–MgO–Al_2O_3–SiO_2–H_2O–HCl. SMPM 78, 225–242.

Matte, P., Maluski, H., Caby, R., Nicolas, A., Kepezhinskas, P.,

Droop, G.T.R., 1993. Geodynamic model and $^{39}Ar/^{40}Ar$ dating for the generation and emplacement of the High Pressure metamorphic rocks in SW Urals. C. R. Acad. Sci. Paris 317 (Serie II), 1667–1674.

McDonough, W.F., Sun, S.-S., 1995. The composition of the Earth. Chem. Geol. 120, 223–253.

Molina, J.F., Poli, S., 2000. Carbonate stability and fluid composition in subducted oceanic crust: an experimental study on H_2O–CO_2-bearing basalts. Earth Planet. Sci. Lett. 176, 295–310.

Montero, P., Bea, F., Gerdes, A., Fershtater, G., Zin'kova, E., Borodina, N., Osipova, T., Smirnov, V., 2000. Single-zircon evaporation ages and Rb–Sr dating of four major Variscan batholiths of the Urals. A perspective on the timing of deformation and granite generation. Tectonophysics 317, 93–108.

Morris, J.D., Leemann, W.P., Tera, F., 1990. The subducted component in island arc lavas: constraints from Be isotopes and B–Be systematics. Nature 344, 31–36.

Mørk, M.B.E., 1985. A gabbro to eclogite transition on Flemsøy, Sunnmøre, Western Norway. Chem. Geol. 50, 283–310.

Pawley, A.R., Holloway, J.R., 1993. Water sources for subduction zone volcanism: new experimental constrains. Science 260, 664–667.

Philippot, P., 1993. Fluid–melt-rock interaction in mafic eclogites and coesite-bearing metasediments: constraints on volatile recycling during subduction. Chem. Geol. 108, 93–112.

Philippot, P., Scambelluri, M., 1995. The composition and behaviour of fluids in high-pressure rocks from the Alps: a review. In: Lombardo, B. (Ed.), Studies on Metamorphic Rocks and Minerals of the Western Alps. A Volume in Memory of Ugo Pognante. Boll. Mus. Reg. Sci. Nat., Torino, vol. 13, pp. 76–101.

Philippot, P., Chevallier, P., Chopin, C., Dubessy, J., 1995. Fluid composition and evolution in coesite-bearing rocks (Dora–Maira massif, western Alps): implications for element recycling during subduction. Contrib. Mineral. Petrol. 121, 29–44.

Plank, T., Langmuir, C.H., 1993. Tracing trace elements from sediment input to volcanic output subduction zones. Nature 362, 739–743.

Poli, S., 1993. The amphibole–eclogite transformation: an experimental study on basalt. Am. J. Sci. 293, 1061–1107.

Poli, S., Schmidt, M.W., 1995. H_2O transport and release in subduction zones: experimental constrains on basaltic and andesitic systems. J. Geophys. Res. 100, 22299–22314.

Pouba, Z., Padera, K., Fiala, J., 1985. Omphacite granulite from NE marginal area of the Bohemian Massif (Rychleby Mts). N. J. Min. Abh. 151, 29–52.

Ringwood, A.E., 1975. Composition and Petrology of the Earth' Mantle McGraw-Hill, New York.

Rubie, D.C., 1990. Role of kinetics in the formation and preservation of eclogites. In: Carswell, D.A. (Ed.), Eclogite Facies Rocks. Blackie, Glasgow, pp. 111–140.

Savelieva, G.N., Nesbitt, R.W., 1996. A synthesis of the stratigraphic and tectonic setting of the Uralian ophiolites. J. Geol. Soc. (London) 153, 525–537.

Savelieva, G.N., Saveliev, A.A., 1992. Relationships between peridotites and gabbroic sequences in the ophiolites o the Urals and the Lesser Caucasus. Ofioliti 17, 117–138.

Scambelluri, M., Philippot, P., 2001. Deep fluids in subduction zones. Lithos 55, 213–227.

Scambelluri, M., Pennacchioni, G., Philippot, P., 1998. Salt-rich aqueous fluids formed during eclogitization of metabasites in the Alpine continental crust (Austroalpine Mt. Emilius unit, Italian western Alps). Lithos 43, 151–167.

Scarrow, J.H., Pease, V., Fleutelot, C., Dushin, V., 2001. The late Neoproterozoic Enganepe ophiolite, Polar Urals, Russia: an extension of the Cadomian arc? Precambrian Res. 110, 255–275.

Schmidt, M.W., Poli, S., 1998. Experimentally based water budgets for dehydrating slabs and consequences for arc magma generation. Earth Planet. Sci. Lett. 163, 361–379.

Schulte, B.A., Blümel, P., 1999. Metamorphic evolution of eclogite and associated garnet–mica schist in the high-pressure metamorphic Maksyutov complex, Ural, Russia. Geol. Rundsch. 87, 561–576.

Selverstone, J., Franz, G., Thomas, S., Getty, S., 1992. Fluid variability in 2 GPa eclogites as indicator of fluid behaviour during subduction. Contrib. Mineral. Petrol. 112, 341–357.

Smulikowski, K., 1967. Eclogites of the Snieznik Mts in the Sudetes. Geol. Sudetica 3, 7–180.

Smulikowski, K., Bakun-Czubarow, N., 1973. New data concerning the granulite–eclogite rock series of Stary Gieraltow, East Sudetes, Poland. Bull. Acad. Pol. Sci., Ser. Sci. Terre 21, 25–34.

Sobolev, N.V., Dobretsov, N.L., Bakirov, A.B., Shatsky, V.S., 1986. Eclogites from various types of metamorphic complexes in the USSR and problems of their origin. In: Evans, B.W., Brown, E.H. (Eds.), Blueschists and Eclogites. Geol. Soc. Am. Mem., vol. 164, pp. 349–363.

Sorensen, S.S., Grossman, J.N., 1989. Enrichment of trace elements in garnet amphibolites from paleo-subduction zone: Catalina Schist, southern California. Geochim. Cosmochim. Acta 53, 3155–3177.

Tatsumi, Y., 1989. Migration of fluid phases and genesis of basalt magmas in subduction zone. J. Geophys. Res. 94, 4697–4707.

Udovkina, N.G., 1971. Eclogites of Polar Urals Nauka, Moscow (in Russian).

Waters, D.J., Martin, H.N., 1993. Geobarometry of phengite-bearing eclogites. Terra Abstr. 5, 410–411.

Wayte, G.J., Worden, R.H., Rubie, D.C., Droop, G.T.R., 1989. A TEM study of disequilibrium plagioclase breakdown at high pressure: the role of infiltrating fluid. Contrib. Mineral. Petrol. 101, 426–437.